TITLE:

Molecular Dynamics Studies of Exothermically Reacting Particle Systems(Dissertation_全文)

AUTHOR(S):

Kawakatsu, Toshihiro

CITATION:

Kawakatsu, Toshihiro. Molecular Dynamics Studies of Exothermically Reacting Particle Systems. 京都大学, 1989, 工学博士

ISSUE DATE:

1989-03-23

URL:

https://doi.org/10.14989/doctor.k4288

RIGHT:

京都大学学術情報リポジトリ
KURENAI 紅
Kyoto University Research Information Repository

新制
工
763
京大附図

Molecular Dynamics Studies of Exothermically Reacting Particle Systems

Toshihiro KAWAKATSU

DECEMBER 1988

Molecular Dynamics Studies of Exothermically Reacting Particle Systems

Toshihiro KAWAKATSU

DECEMBER 1988

Molecular Dynamics Studies of Exothermically Reacting Particle Systems

by

Toshihiro KAWAKATSU

Submitted in partial fulfilment of the
requirement for the degree of
DOCTOR OF ENGINEERING
(Applied Mathematics and Physics)
at
KYOTO UNIVERSITY
Kyoto, Japan
DECEMBER 1988

ABSTRACT

Various nonequilibrium phenomena in an exothermically reacting system are studied with use of the molecular dynamics (MD) method. The model reaction system is a hard disk system in which an exothermic isomerization reaction expressed as $A + S \underset{\leftarrow}{\overset{\rightarrow}{}} B + S + \Delta Q$ is introduced as the two body collisions between the hard disks. Here, ΔQ is a reaction heat of the forward reaction and the species S plays a role of a catalyst.

We performed the MD experiments on the relaxation process from the initial nonequilibrium state in which the A and the S particles are uniformly distributed. During such relaxation processes, the A particles turn to the B particles through the reaction $A + S \rightarrow B + S$ and the created B particles form the spatial patterns. Two types of the pattern formation processes which are similar to those found in the phase transition phenomena of the alloy or the spin systems are examined. One is a nucleation and growth process of the circular domain of the created B particles and the other a spatially homogeneous creation of the B particles which resembles to the spinodal decomposition. The former corresponds to the ignition and the propagation of the reaction wave and the latter to the thermal explosion, respectively. The growth law of the circular domain in the former case is investigated and the differences between our reacting system and the alloy or spin systems are discussed.

In order to clarify the propagation mechanism of the boundary of the above-mentioned nucleus in detail, the MD

experiments on the one-dimensional propagation phenomena of the reaction wave are performed. It is found that the reaction wave in our system corresponds to a detonation and the MD results on the structure and the propagation velocity of the detonation well reproduce those of the real detonation as long as there exists enough number of the catalyst S. The spatial correlation effects on the detonation propagation mechanism are studied by changing the molar fraction of the S particles in the initial state. For the case of the high molar fraction of the A particles in the initial state, we found that the effects of the spatial inhomogeneity in the microscopic level become to be dominant in the propagation mechanism. The energy relaxation processes at the detonation wave front are investigated in order to clarify such effects. We found that the decay process of the fluctuations in the spatial distribution of the particles is the rate-determining process in the energy relaxation process behind the detonation wave front.

Next, we investigated above-mentioned spatial inhomogeneity effects by performing a series of MD runs of relaxation processes from the initial homogeneous states composed of the A and the S particles. The decaying law of the number of the A particles are found to be different from that predicted by the rate equation which assumes the spatial homogeneity and the late stage dynamics is dominated by the initial fluctuations in the spatial distribution of the particles.

Finally, we performed the MD experiments on the detonation propagation in the $A \underset{\leftarrow}{\overset{\rightarrow}{}} A^* \underset{\leftarrow}{\overset{\rightarrow}{}} B$ type reaction system in order to

clarify the effects of the activated complex A^* with finite lifetime. The existence of the A^* does not change the propagation mechanism but changes the wave front structure slightly. This result indicates that the model reaction system $A + S \underset{\leftarrow}{\overset{\rightarrow}{}} B + S$, which neglects the lifetime of the activated complex A^*, used in our MD experiments is a good approximation of the real reaction system as long as we are concerned with the high-speed nonequilibrium processes such as the detonation and the explosion phenomena.

ACKNOWLEDGEMENTS

The author would like to express his sincere gratitude to Professor Akira Ueda, Department of Applied Mathematics and Physics, Kyoto University, for his guidance, discussions, encouragements and critically reading the manuscript. He also expresses his deep thanks to Dr. Toyonori Munakata, Department of Applied Mathematics and Physics, Kyoto University, for valuable discussions and encouragements. He wishes to express his sincere gratitude to Professor Kyozi Kawasaki, Department of Physics, Kyushu University, for his encouragements.

Several helpful discussions with Dr. Akito Igarashi, Dr. Yuji Ishimori, Mr. Yutaka Kaneko and Mr. Takashi Matsuda, Department of Applied Mathematics and Physics, Kyoto University, Mr. Kazuhiro Fuchizaki, Faculty of Engineering Science, Osaka University, Dr. Ken Sekimoto and Mr. Hisao Hayakawa, Department of Physics, Kyushu University, are gratefully acknowledged.

Most of the computations were done on the FACOM M-380 and VP-200 computers of the Computer Center of the Institute of Plasma Physics and the FACOM M-780 computer of the Data Processing Center of the Kyoto University.

CONTENTS

CHAPTER I

INTRODUCTION

§ 1.1 Overview

Recently, there has been taken a great interest on the dynamical phenomena occurred in the various chemical reaction systems. Typical examples are the photochemical processes in the liquid solvent,[1] the macroscopic cooperative phenomena in the nonlinear and nonequilibrium systems,[2] the combustion and the explosion in the exothermically reacting systems[3,4] and the fluctuation dominated kinetics in the diffusion controlled reaction systems.[5] The most difficult point in treating these phenomena theoretically is the fact that the system is in far from equilibrium state. In these cases usual macroscopic description of the system using the deterministic differential equations is insufficient to understand the phenomena in detail and the microscopic fluctuations must be taken into account.

The molecular dynamics (MD) method is a computer experiment technique which can investigate both the static and the dynamic processes of the system including the microscopic fluctuations. This method was first applied to the dynamics of the simple gases, liquids and solids from the end of the 1950's to the 1960's.[6-11] As the full description of the chemically reacting systems in far from equilibrium state is required in order to treat the fluctuations of various types and scales, the use of

the MD method in these fields is expected to provide a new aspect to our knowledge on the reaction systems. In addition, we can mention another advantage of the MD method. By using the MD method, we can investigate not only the realistic systems but also the idealized systems in which the particles interact each other with an idealized interaction. We can expect that the universal features over the reacting systems can be obtained with a simplified model which retains the essentials of the reacting systems. In the following, recent developments of the MD experiments on the dynamical phenomena of the chemically reacting systems are reviewed.

The chemical reaction phenomena that the MD method was first applied are the photo-chemical processes.[12-16] As the photo-chemical processes are often accompanied by the release or the absorption of a large amount of chemical energy, these processes produce a very far from equilibrium state. The photo-dissociation and the recombination of molecules in a liquid solvent is employed frequently as an example of such processes. Bunker and Jacobson studied the cage effect on the photo-dissociation and recombination of the I_2 molecule in liquid CCl_4 solvent using the MD method.[12] The electron which is initially in the ground state of the I_2 molecule is activated to the excited state by the photon absorption and then the I_2 molecule begins to dissociate into two I atoms with releasing the binding energy to the solvent molecules. As this process takes place in the surrounding solvent molecules, the situation is as if the two I atoms were trapped in a cage constructed by the solvent

molecules. This cage prevents the dissociated I atoms pair from getting apart and raises the possibility of the recombination of the I atoms back into the I_2 molecule. The MD experiments of Bunker and Jacobson showed that the recombination process is strongly affected by the cage effect and the microscopic description of the system is needed to understand the recombination process entirely.

In the 1970's, Prigogine and his co-workers have developed the theory of "dissipative structures". The dissipative structures are the macroscopic cooperative phenomena occurred in the chemical reaction systems such as the bifurcation, the emergency of the spatial and/or temporal oscillations and so on.[2] The usual description of the dissipative structures is done with use of the macroscopic reaction-diffusion equations, which describe the diffusive motion of the macroscopic variables, such as the number density of the chemical species or the temperature, taking into account of the reaction processes. It is shown that the dissipative structures can emerge only in the case that the reaction-diffusion equation of the system is nonlinear with respect to its dependent variables and the system is in nonequilibrium state, which is often called as the "nonlinear nonequilibrium system". The main target of the theory of dissipative structures by Prigogine et al. was the nonlinear non-exothermic reaction systems.

In the transient period before such cooperative phenomena emerge, many types of fluctuations compete and a specified mode grows to a macroscopic scale to dominate the dynamics of the

whole system and leads the system to the cooperative regime. In such early stage, both the macroscopic and the microscopic fluctuations coexist in the system. It was demonstrated that the macroscopic fluctuation is well described by the birth-and-death theory and obeys the non-Poisson distribution. However, the birth-and-death theory takes into account of only the large scale fluctuations and it neglects the small size fluctuations. It was theoretically predicted that the small size fluctuations do not obey the non-Poisson distribution but obey the Poisson one.[17-20] The first attempt to examine this problem directly with use of the MD method was done by Portnow in 1975.[21] Portnow performed the MD experiments on the reacting hard sphere systems and calculated the probability distribution of the small fluctuations in the number density of each of the species. The results of this work support the theoretical prediction of the Poisson behavior of the small fluctuations. Therefore, the characteristics of the large fluctuations are different from those of the small fluctuations and it is required to treat the evolution of the macroscopic variables along with the microscopic fluctuations simultaneously in discussing the initiation of the dissipative structures. Stimulated by the above Portnow's work, several MD experiments were performed on the chemical phase transition and other dynamical problems of the chemically reacting systems[22-28]

While the cooperative phenomena in the non-exothermic reaction systems originate from the nonlinearity of the reaction-diffusion equations, in the exothermic reaction systems the

cooperative phenomena are derived from the nonlinearity in the Arrhenius factor of the reaction rate constant of the form $\exp(-\varepsilon/k_BT)$, where ε is the activation energy of the reaction, k_B is the Boltzmann's constant and T is the temperature. As the exothermic reactions cause the temperature raise, such nonlinearity gives the reaction a self-catalytic feature and the region where the exothermic reactions proceed spreads automatically. This process is essential in the combustion and the explosion phenomena.[3,4] As the combustion and the explosion phenomena are accompanied by the release of a large amount of heat, the temperature and the pressure of the system change drastically in a very short time period and/or in a very small distance. By this reason, the MD experiments on such phenomena as well as the theoretical analyses have been difficult to be performed. Until recently the combustion and the explosion phenomena have been studied using the hydrodynamic equations based on the continuum approximation.[3,4] Whether the continuum approximation to the combustion phenomena is appropriate or not is an important problem. Very recently, the MD experiments on this problem become to be performed. Tsai and Trevino investigated the dynamics of the exothermic reactions by MD method in a series of their works.[29-31] Using the three-dimensional model of the exothermically reacting system composed of the energetic diatomic molecules, they studied the nonequilibrium relaxation processes,[29] the equilibrium properties[30] and the detonation propagation phenomena[31] in crystals. Here the detonation, which will be explained in detail

in the following chapters, is a kind of the combustion wave accompanied by a shock wave and it propagates with a supersonic velocity. The detonation propagation phenomena was also investigated by Peyrard et al. for the 2-dimensional energetic diatomic molecular crystal,[32] by Lambrakos for the 3-dimensional crystals[33] and by Kawakatsu et al. for the 2-dimensional high-density liquids.[34-37] On the other hand, the microscopic properties of the combustion and the thermal explosion processes are studied by Chou and Yip,[38-39] by Gorecki and Gryko[40] and by Kawakatsu and Ueda[41] using the MD method. From these works, the precise microscopic information on the detonation, the combustion and the explosion phenomena beyond the continuum approximation have been accumulated and more detailed understanding of such phenomena has been achieved. The details will be mentioned in the following chapters.

The problem on the effects of the fluctuation in the spatial distribution of the particles on the dynamics of the diffusion controlled reaction systems becomes to gain attentions of many researchers in the last decade.[5,42-50] When the time scale of the elementary processes of the reaction is much shorter than that of the intervals of the contacts of the reaction pair by diffusive motion, the reaction is called as diffusion controlled. In such case, the spatial inhomogeneity, such as the clustering of the particles, plays an important role in the late stage dynamics through the diffusion process. Among many types of diffusion controlled reactions, the radical recombination reaction $A + A \rightarrow 0$,[5,42] the particle-antiparticle recombination

reaction $A + B \rightarrow 0$[5,42-46] and the unimolecular trapping reaction $A + S \rightarrow S$[47-49] have been extensively studied by the theoretical and the Monte Carlo simulation method. In chapter V, it will be shown that our model reaction system can be reduced to the unimolecular trapping reaction type and the results of our MD experiments on the fluctuation dominated kinetics will be compared with those of the theoretical and the Monte Carlo results of the previous works.

§ 1.2 Outline of the Dissertation

The thesis is composed of 5 parts which are concerned with the following five topics: 1) The model reaction systems and the technical details of our MD experiments, 2) the spatial pattern formation processes in the exothermically reacting systems, 3) a detonation propagation phenomena (the structure and the propagation velocity) and the energy relaxation processes at the detonation wave front, 4) the fluctuation dominated kinetics on the diffusion controlled reaction and 5) the effects of the activated complex with finite lifetime on the reaction dynamics. All of these investigations are performed on the 2 dimensional hard disk system combined with the model exothermic isomerization reaction $A + S \underset{\leftarrow}{\overset{\rightarrow}{}} B + S + \Delta Q$ (ΔQ is the reaction heat of the forward reaction) by the MD computer experiments.

In the first part (chapter II), detailed explanations on the model system and the techniques used in our MD experiments are

presented. Our model reaction system is a very simple one. Why we decided to use such a simple model and what features of the reaction systems we expect to understand are explained in detail. The computational techniques for the MD method are also presented.

From the second to fifth parts are devoted to the results of our MD experiments. In the second part (chapter III), we study the spatial pattern formation processes by the created B particles during the relaxation from the nonequilibrium initial state composed of uniformly distributed A and S particles. We will find two types of pattern formation processes, one is a nucleation and growth of the circular domain of the created B particles and the other is a homogeneous creation of the B particles. These correspond to the ignition and the thermal explosion processes, respectively. The analogy of these processes to the phase transition phenomena of the alloy or spin systems is discussed.

The third part (chapter IV and V) is devoted to the investigations of the detonation propagation phenomena. It is shown that our simple reaction model, which is a hard disk model combined with an exothermic reaction, can reproduce the main features of the real detonation concerning such as the wave front structure and the propagation velocity. A cage effect, which is the result of the spatial fluctuations in the particle distribution, on the detonation propagation phenomena is also studied in detail by calculating the energy relaxation processes at the detonation wave front. It will be shown that in the case

of small molar fraction of the catalyst S the energy relaxation processes are dominated by the cage effect in the late stage and therefore the long time behavior is quite different from that predicted with use of the assumption of spatial homogeneity. We can recognize that the fluctuation in the molecular level finally affects the macroscopic phenomena such as the detonation propagation in the late stage.

In the fourth part (chapter VI), the effects of the fluctuations in the particle distribution on the macroscopic dynamics of the system in the late stage are investigated by calculating the relaxation process of the particle number from the initial nonequilibrium state composed of the A and the S particles. The decay law of the number density of the A particles does not depend on time t as exp(-kt) predicted by the rate equation (assumption of homogeneity) but as $\exp(-kt^{1/2})$. The comparison between the statistical theory and the MD experiments are presented.

In the final part (chapter VII), the activated complex with finite lifetime which has been neglected in the studies in the second to fourth parts is taken into account to test the range of validity of our model and the effects of the activated complex on the dynamical processes of the reaction system. As the objective phenomena, we adopt the detonation propagation phenomena. It will be demonstrated that the role of the activated complex is not essential in the detonation propagation mechanism except for the slight change observed in the detonation wave structure.

CHAPTER II

DETAILS OF THE MODEL FOR THE MD EXPERIMENTS

§ 2.1 General Procedures of the MD Experiment

In the field of statistical physics there are two major techniques for the computer experiments, one is the MD method and the other the Monte Carlo (MC) method. Basically the MC method is a technique to calculate the canonical ensemble average of the physical quantities in the equilibrium state.[51,52] In the MC experiments, a lot of representative points in the phase space or the configuration space are generated by the Markoffian random walks in such a space and the ensemble average is taken over all these representative points. So the MC method is suitable to investigate the static properties of the system in its equilibrium state. On the other hand the MD method is a useful tool to study the dynamical properties of the system such as the transport phenomena, non-equilibrium phenomena and so on.[52] In the MD calculations, for the system consisting of many interacting particles, the Newton's equations of motion (EOM) for each of the particles

$$m_i \frac{d^2 \vec{r}_i(t)}{dt^2} = - \frac{\partial \Phi(\{\vec{r}_j(t)\})}{d\vec{r}_i} \qquad (2.1.1)$$

are integrated numerically to follow the time evolution of the system. Here, m_i and $\vec{r}_i(t)$ is the mass and the position of the i-th particle at time t and Φ is the total interatomic potential energy defined as

$$\Phi(\{\vec{r}_j(t)\}) = \frac{1}{2} \sum_j \sum_{k(\neq j)} \phi\,(|\vec{r}_j - \vec{r}_k|), \qquad (2.1.2)$$

where we approximated the total potential Φ as the sum of the pair interaction potential $\phi(r)$. From the data thus obtained the dynamical quantities are calculated.

The selection of the interatomic potential function $\phi(r)$ is the most important problem in the MD experiments. The commonly used potential functions are classified in two types; One is the continuous potential functions such as the Coulomb potential $\phi(r) = k/r$, the Lennard-Jones potential $\phi(r) = 4\varepsilon\,((\frac{\sigma}{r})^{12} - (\frac{\sigma}{r})^{6})$ and the soft core potential $\phi(r) = \varepsilon(\frac{\sigma}{r})^{n}$, where σ corresponds to the diameter of the particle and k and ε are constants. The other type of the interatomic potentials are discontinuous potentials such as the hard core potential

$$\Phi(r) = \begin{cases} 0 & (r > \sigma) \\ \infty & (r \leq \sigma) . \end{cases} \qquad (2.1.3)$$

For the continuous potential function, Verlet's leap-flog algorism

$$\vec{r}_i(t+\Delta) = 2\,\vec{r}_i(t) - \vec{r}_i(t-\Delta) + \frac{\Delta^2}{m_i}\left[- \frac{\partial \Phi}{\partial \vec{r}_i} \right] + o(\Delta^4) \qquad (2.1.4)$$

is usually employed to integrate EOM, where Δ is the time mesh width. For the hard core potential, the integration of the EOM are performed in a quite different manner. As the interaction between the hard core particles is non-zero only when the two particles contact, the track of a particle between consecutive two collisions draws a straight line. Therefore we have only to determine the successive collision events in order to grasp the whole behavior of the system.

In §.2.3, the detailed procedure is given for the MD experiments on our model system which consists of the particles interact with the hard core potential.

§ 2.2 Model of the Reaction System

Our model system for the MD experiments consists of N hard disks, all with the identical mass m and the diameter σ, contained in a square/rectangular box. Each disk is assigned one of the three species A, B and S. We assume that an exothermic isomerization reaction, $A + S \underset{\leftarrow}{\overset{\rightarrow}{}} B + S + \Delta Q$, takes place on a two-body collision between the two disks. Here the quantity ΔQ is the reaction heat of the forward reaction. Therefore, the potential energy (chemical energy) of an A particle is higher than that of a B particle by the amount of ΔQ. We assume that there exist a transition state between these two isomers A and B and the barrier hight of the transition state, which corresponds to the so-called activation energy, is assumed to be ε for the forward reaction and ε + ΔQ for the reverse reaction. We further assume that the lifetime of such transition state is negligibly short and the reaction A → B or B → A takes place instantaneously. If a reactive pair of particles (A + S or B + S) collides and the head-on collision component of the relative kinetic energy exceeds the activation energy (ε for the forward reaction and ε + ΔQ for the reverse reaction), this collision is regarded as reactive. Then the particle A (B) changes to B (A) and the total kinetic energy increases by ΔQ for the forward reaction A + S → B + S and decreases by ΔQ for the reverse reaction B + S → A + S. The velocities of the colliding particles after the collision are perfectly determined by the momentum conservation law and the energy conservation law that

takes into account of the energy release or the energy absorption of the reaction heat. As every particle has the identical mass, the released energy is divided equally between the two colliding particles in the center-of-mass system. If the above-mentioned conditions for the reactive collision are not fulfilled, then the collision is regarded as non-reactive and elastic. Here, for simplicity, we assume that any type of collision other than A + S and B + S, such as A + A, are elastic. This assumption, however, is expected not to affect the qualitative features that we are now interested in.

In this model, we adopt only three characteristic properties which are basically common in reacting systems, that is; a) the change of chemical species, b) the release or the absorption of the reaction heat and c) the translational freedom of the particles. All the other properties except a)-c) are neglected in this model. Our main purpose is to extract the common features of the reacting system by using the above-mentioned simplified model. It can be said that the features which this model reaction system shows are universal in the general reaction system. In the following we study this model reaction system by the MD method from such point of view.

§ 2.3 Computational Schemes

In this section the computational scheme for our MD experiments are presented.

Let $\vec{r}_i$ and $\vec{v}_i$ be the position and the velocity of the i-th particle. We define the relative position and the relative velocity of the j-th particle from the i-th particle as

$$\vec{r}_{ij} = \vec{r}_j - \vec{r}_i \tag{2.3.1}$$

and

$$\vec{v}_{ij} = \vec{v}_j - \vec{v}_i \ . \tag{2.3.2}$$

If we define b_{ij} as

$$b_{ij} = \vec{r}_{ij} \cdot \vec{v}_{ij} \ , \tag{2.3.3}$$

the two particles i and j collide only when $b_{ij} < 0$ and $b_{ij}^2 - |\vec{v}_{ij}|^2 (|\vec{r}_{ij}|^2 - \sigma^2) > 0$. (Note that each particle moves straight between the collisions.) Then the time spent until the collision between i and j takes place is given by

$$t_{ij} = [\, -b_{ij} - \{b_{ij}^2 - |\vec{v}_{ij}|^2 (|\vec{r}_{ij}|^2 - \sigma^2)\}^{1/2}\,] / |\vec{v}_{ij}|^2 . \tag{2.3.4}$$

The velocities of the colliding two particles i and j after the collision, $\vec{v}'_i$ and $\vec{v}'_j$, are determined using the momentum and the energy conservation relations as follows:

$$\vec{v}'_i = \vec{v}_i - \Delta v \cdot \vec{e} \qquad (2.3.5)$$

and

$$\vec{v}'_j = \vec{v}_j + \Delta v \cdot \vec{e} \ . \qquad (2.3.6)$$

Here $\vec{e}$ is the relative position $\vec{r}_{ij}$ at the instant of the collision and Δv is given by

$$\Delta v = \frac{1}{2} \left[- v_{r//} + \left(\frac{4}{m} \left(E_{r//} + q \right) \right)^{1/2} \right] \ . \qquad (2.3.7)$$

In eq. (2.3.7), q is the reaction heat which is equal to ΔQ for the forward reaction A + S → B + S, $-\Delta Q$ for the reverse reaction B + S → A + S and 0 for the non-reactive collisions. The quantities $v_{r//}$ and $E_{r//}$ are the head-on collision components of the relative velocity and the relative kinetic energy, respectively, defined as follows:

$$v_{r//} = \vec{v}_{ij} \cdot \vec{e} \qquad (2.3.8)$$

$$E_{r//} = \frac{m}{4} \cdot v_{r//}^{\,2} \ . \qquad (2.3.9)$$

On the collision between the reactive type pair, the collision is regarded as reactive if $E_{r//}$ exceeds the activation energy of the

reaction. Otherwise the collision is regarded as non-reactive and therefore elastic as mentioned before.

In order to save computing time for the calculation of the successive collisions, we employ the book-keeping method. This method is based on the fact that in a dense system a particle collides only with its neighbouring particles within a short time interval. At $t = n\ t_B$ $(n = 0,1,2,\cdots\cdots)$, a table is made for each of the particles which registers the indices of all the particles locating within the distance r_B from the particle, where the time t_B and the distance r_B must be determined appropriately by taking the following situation into account. In the time interval $n\ t_B \leq t \leq (n+1)\ t_B$, as the candidates of possible collisions, only pairs registered at $t = nt_B$ are considered. No collisions occur between particle pairs which have not been registered in the table may take place. As the result the cost for searching collision events is reduced largely.

To find the fist collision in the system, we calculate the collision times for all the particle pairs registered in the table under the assumption that each particle moves straight with its velocity without colliding. The obtained collision times are registered in a 1-dimensional list in a descending order. As the first element of this list corresponds to the first collision in the system, we make each particle travel until the time and the velocities of the colliding two particles are renewed according to eqs. (2.3.5) and (2.3.6). Then the data in the list of collision times which concern to the colliding pair are also

renewed and the renewed data in the list are sorted. In these way we can trace the time evolution of the system.

CHAPTER III

PATTERN FORMATION PROCESSES IN THE EXOTHERMICALLY REACTING SYSTEMS

§ 3.1 Introduction

The pattern formation processes in the various chemical as well as physical systems have recently been one of the central interests in the fields of statistical physics and the physical chemistry, and a lot of works have been done on the phase transition phenomena, chemical instability, hydrodynamic instability and so on.[2,4,53,54] On the emergence of such spatial patterns, it is well known that the fluctuations play an essential role.[2,53,54] Therefore the MD method, which treats the microscopic fluctuations exactly, can give us an important information on such phenomena. Until recently, however, the MD method was not applied to the pattern formation processes because of the limitation of the system size available on the computers. Only recently, the MD method becomes to be applied to the nucleation processes in the chemical phase transition[23,26] and the hydrodynamic instability.[55] In the present chapter, our main concern is the pattern formation processes in the exothermically reacting systems and we study the relation between these macroscopic patterns and the microscopic dynamics of the particles.

§ 3.2 Results of the MD Experiments

The model reaction for the MD experiments are exothermic reaction $A + S \underset{\leftarrow}{\overset{\rightarrow}{}} B + S + \Delta Q$ explained in the preceding chapter. For investigating the pattern formation processes, MD experiments are performed as follows: First, we prepare a non-reactive hard disk system in thermal equilibrium of temperature T_0 contained in a square box with the periodic boundary condition on each of the sides. Next, we assign species to each particle randomly, with a uniform density distribution, in such a way that a half of the total number of particles are A's and the rest are B's. Since an A particle has more internal energy than a B particle, the state then changes to a nonequilibrium state that has an excess internal energy. We adopt this state as an initial state of the reacting system. Then, we follow the time evolution of this system under the exothermic reaction dynamics. The system is expected to relax towards an equilibrium state of temperature, say T_e, in which the numbers of A and B particles, N_A and N_B, satisfy the relation $N_A/N_B = \exp(-\Delta Q/k_B T_e)$. We set the total number of particles $N = 9752$ and the density of the particles $n\sigma^2 = 0.770$, where n is the total number density and σ the diameter of the hard disk. This density corresponds to a fluid state of density slightly lower than its fluid-solid transition density.[7] Parameters ΔQ and ε are selected in two ways: that is, a) $\Delta Q = 40.0$ and $\varepsilon = 10.0$; and b) $\Delta Q = 3.0$ and $\varepsilon = 3.0$. Here the parameters ΔQ and ε are measured by the mean kinetic energy per particle of the initial state. Computations are continued until

200,000 collisions have been performed in the system. Hereafter, we make quantities dimensionless by use of the units of length σ, mass m (m: mass of the hard disk) and time $(m\sigma^2/k_BT_0)^{1/2}$, respectively.

In Figure 3.1 we show the time evolution of the spatial distribution of the created B particles through reactions for cases a and b, respectively. In case a, we observe clearly a nucleation and growth process of the circular domain of the B particles which corresponds to the ignition and combustion process. Case b shows a rapid and almost homogeneous growth of the domains of B particles, which is suggestive of spinodal decomposition in the phase separation of alloys. We remark here that the initial state is metastable in case a, while unstable in case b. In case a, as the activation energy ε is much higher than the average kinetic energy of a particle, most of the collisions are elastic. Once a reaction takes place, however, a large amount of energy is released, which raises the local temperature and causes reactive collisions successively. Therefore this state may be considered as metastable. On the other hand, in case b, as the activation energy is relatively low, reactive collisions can take place easily and the system relaxes to the equilibrium state rapidly. So this state is unstable. These circumstances are similar to those of alloy or spin systems.[56)]

For case a, we carried out 5 runs in order to get qualitative features for the growth mechanism of the nucleus. In these runs, we assign initially an excess kinetic energy to an A particle at

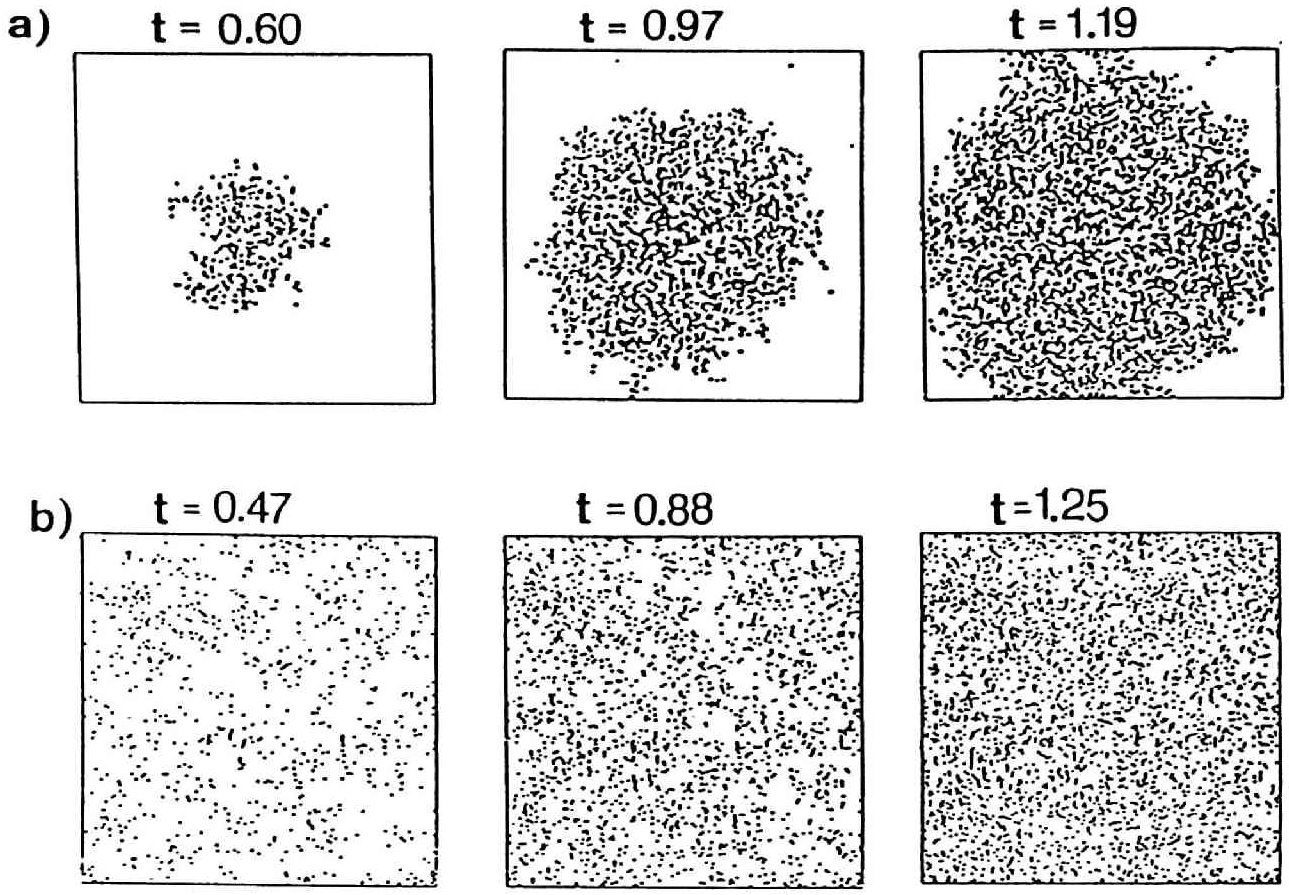

Figure 3.1

Time evolutions of the spatial distribution of the created B particles are shown for case a and case b, respectively.

the center of the system so as to reduce the initial induction time before the ignition, with which we are now less concerned. In Fig. 3.2, we show the time evolution of the radius of the nucleus. Here, the radius of the nucleus is defined as the radius of a circle centered at the initial ignition point that contains 90% of the created B particles. We see that the radius evolves proportionally to time throughout the computations. Figure 3.3 shows the time evolution of the profile of the domain, that is, the radial distribution of the B particles measured from the initial ignition point. To derive the profile, which is obtained by averaging over the 5 runs, the origins of time of individual runs are suitably shifted in order to reduce the effects of fluctuation in the induction time.

Two types of mechanism can be considered for this linear growth of the domain. One is the mechanism of thermal diffusion and activation at the domain boundary, which is well known for the drift mechanism of the flame and leads to the stationary propagation of the boundary.[3,4] However, as is shown in Fig. 3.3, the profile of the domain boundary has not yet reached its stationary profile. In this time region, therefore, a different mechanism is required to explain the growth mechanism. In Fig. 3.4, we present a flow pattern of the momentum field which is indicated by arrows. Here, the system is divided into 20×20 meshes with a mesh width of 5.5σ. An arrow is defined as an average momentum of about 80 particles contained in a small circle centered at a mesh point with a radius same as the mesh width. There exists a circular domain in Fig. 3.4, and the

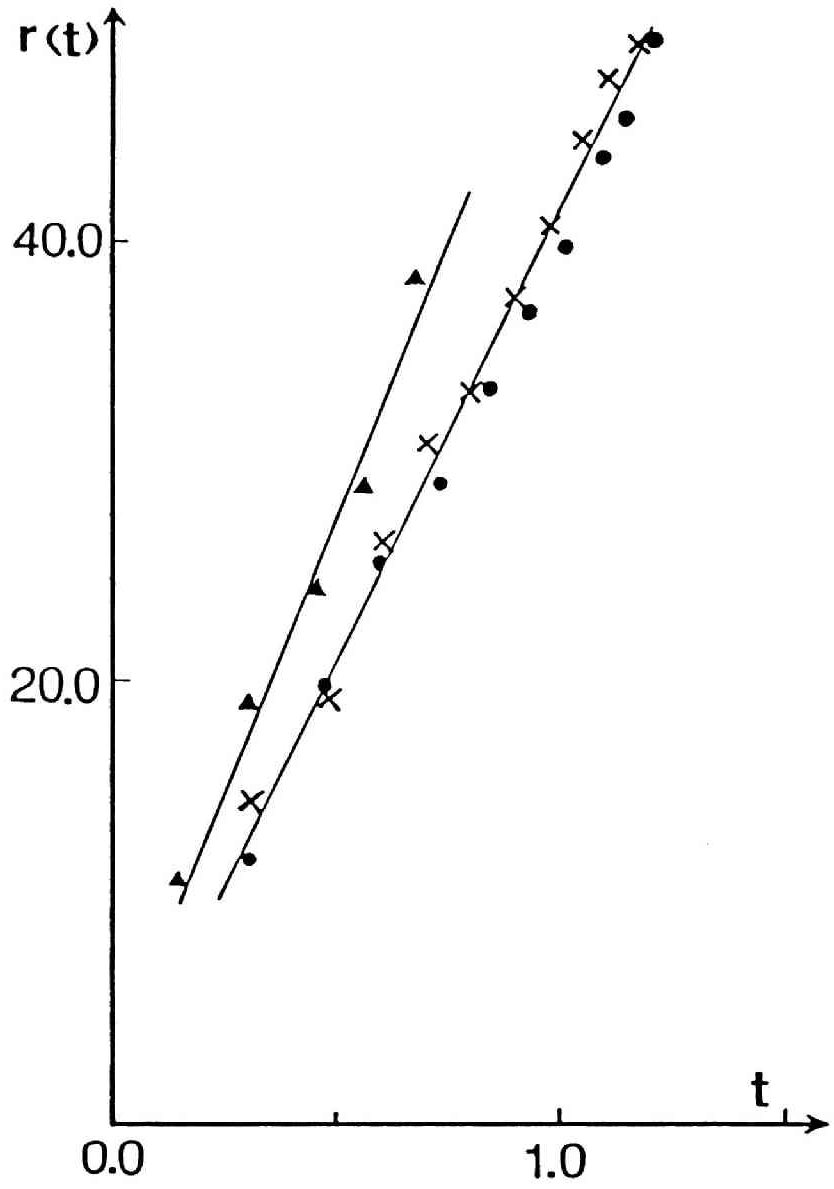

Figure 3.2

Increase of the radius of the domain of the created B particles with time is shown for 3 runs (o , Δ and ×) for case a.

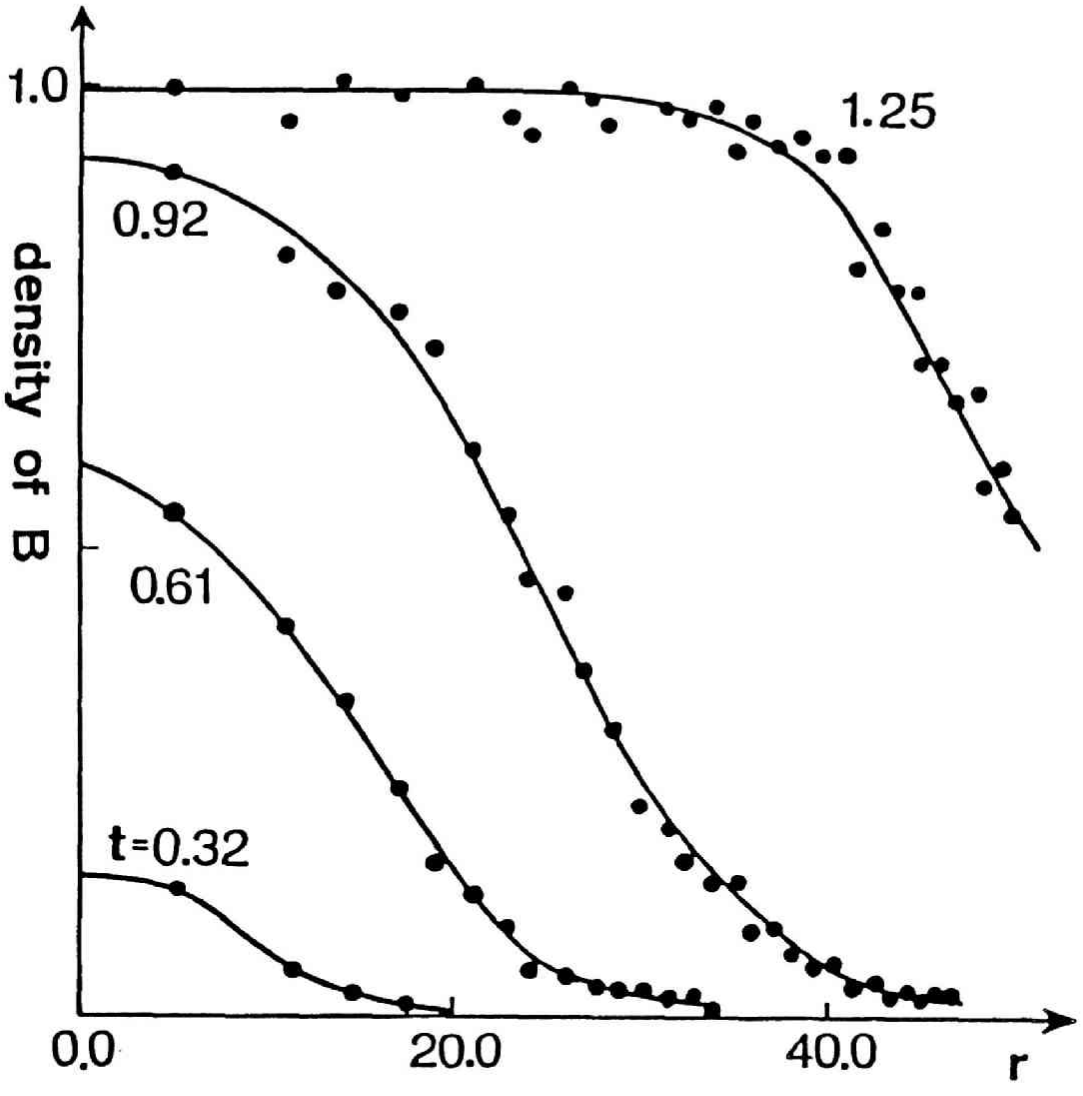

Figure 3.3

The profiles of the domain which are represented by the radial density distribution of B particles at time t=0.32, 0.61, 0.92 and 1.25 measured from the ignition time are shown for case a.

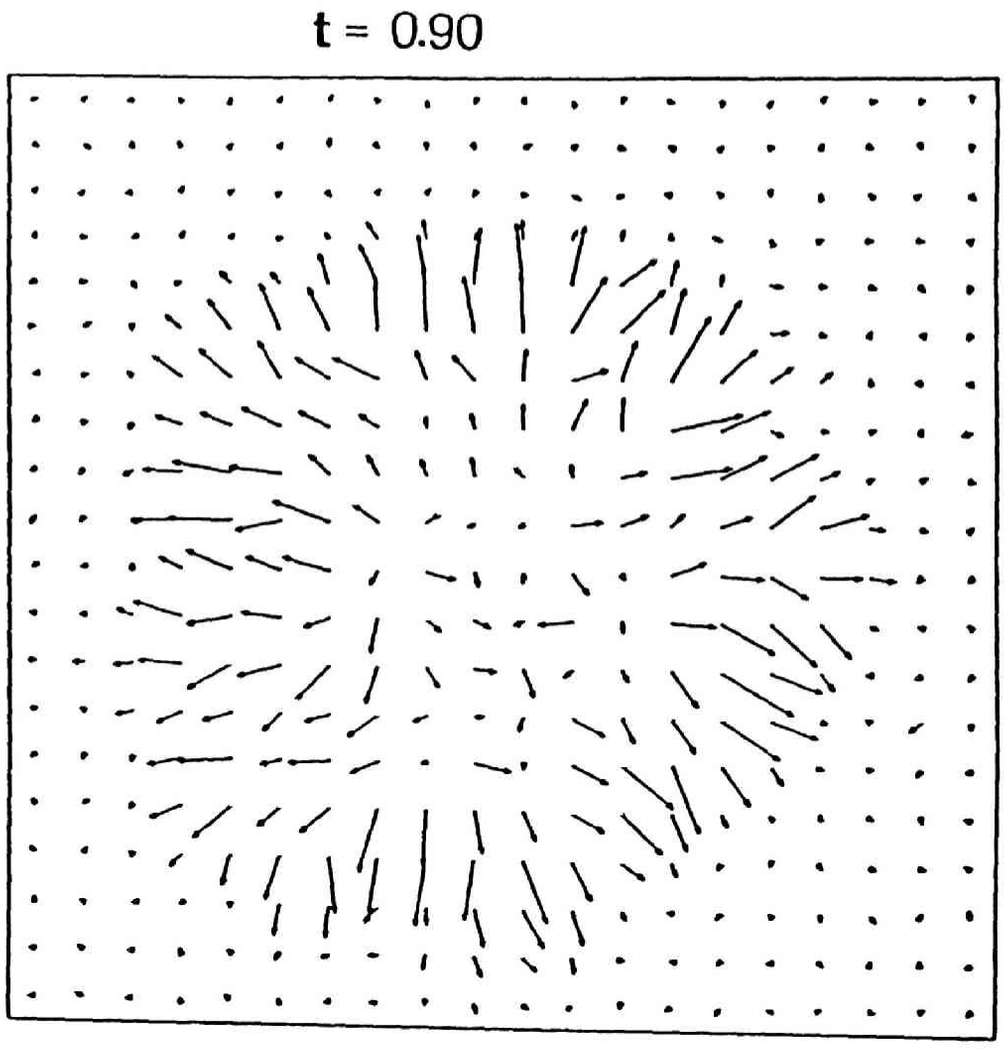

Figure 3.4

A snapshot of the momentum flow pattern at the early stage of the nucleation and growth process (t = 0.90) is shown for case a.

momentum flow is noticeable in a boundary region of this domain with a width of about 15σ. The domain previously defined by B particles in Fig. 3.1 is well reproduced by this domain of momentum flow. Since successive collisions of particles at the domain boundary quickly transfer the momentum out and away from the domain, this momentum transfer is expected to dominate the spreading of the domain. If the momentum flux at the boundary flows steadily, the boundary propagates with a constant speed. For the duration of the stationary propagation, balancing is needed between the decay of momentum flux at the boundary and the supply of momentum due to the exothermic reactions and the increase of pressure inside the domain. The stability of this balancing and the transition from the momentum transfer mechanism to the thermal diffusion mechanism are interesting problems from the viewpoint of the dynamical correlation. These problems will be discussed in the following chapters.

CHAPTER IV

DETONATION WAVE: PROPAGATION VELOCITY AND STRUCTURE

§ 4.1 Introduction

In the preceeding chapter (chapter III), we studied the pattern formation processes of a hard disk system which undergoes an exothermic reaction. We found that this model system shows spatial pattern formation processes similar to those in the phase transition of the alloy system, that is, a nucleation and growth process and a uniform pattern formation like a spinodal decomposition. We studied the nucleation and growth process and found that the boundary of the nucleus, which corresponds to a combustion wave, propagates steadily in time and that the wave is driven by the fast flow of momentum around the boundary region. In this chapter, we study the structure of this reaction wave and the mechanism of the propagation in detail by performing the MD experiments of the one-dimensional propagation of the reaction wave for a long period. The results of such MD experiments will be also used to test the validity of the macroscopic description of reacting system by the macroscopic equations.

In § 4.2, the details of our experiments are presented. An analysis by the macroscopic hydrodynamic theory is made for our MD experiments in § 4.3. Comparison between the hydrodynamic theory and the MD experiments is made in § 4.4. We will see that the reaction wave of our experiment corresponds to a detonation. Finally in § 4.5, we summarize our results.

§ 4.2 Model Reaction and MD Experiment

The model reaction system used in the present experiment is basically the same as that used in chapter III. The system consists of N hard disks each of which has one of the chemical species A, B and S and all disk have the identical mass m and the diameter σ. An exothermic isomerization reaction denoted as;

$$A + S \underset{\leftarrow}{\overset{\rightarrow}{}} B + S + \Delta Q \qquad (4.2.1)$$

$$(\Delta Q \geq 0)$$

is introduced into this system.

In this chapter, the dynamics of one-dimensional propagation of a reaction wave is studied. To observe the wave propagation for a long period, we prepare a rectangular box whose side length L_x in the x-direction and the side length L_y in the y-direction are in the ratio 20 : 1. We impose a periodic boundary condition upon the sides in the x-direction while we assume the both sides in the y-direction as the elastic walls. A reaction wave is

generated in the vicinity of one end of the side in the x-direction (x = 0) and travels along the x-direction.

The computations are performed as follows: First, we prepare a hard disk system in thermal equilibrium of temperature T_0. Next, each particle is given species A or S randomly in such a way that the half of the total particles are A's and the rest are S's. As was shown in chapter III, this state is metastable in case that the activation energy ε is large compared to the mean kinetic energy per particle $k_B T_0$. To initiate the reaction, we heat the particles in a small region at the one end of the system ($0 \leq x \leq L_x/50.0$) by multiplying a factor 5.0 to their velocities. Then we can observe a reaction wave propagating along the x-direction.

Hereafter, we use dimensionless quantities by use of the units of length σ, mass m, time $(m\sigma^2/k_B T_0)^{1/2}$ and energy $k_B T_0$.

We performed a series of MD runs for a various values of the number density of the particles $n\sigma^2$ (n : total number density), reaction heat ΔQ and activation energy ε. Their values are listed in Table 4-I. For the runs of type α) in Table 4-I, we changed the $n\sigma^2$ keeping ΔQ and ε to be constant, while we changed ΔQ and ε keeping $n\sigma^2$ to be constant for type β) runs. All runs were performed for 9,000 hard disk system. For each set of parameters of type α) given in Table 4-I, three runs were performed changing the initial configurations and velocities of particles and the assignment of species. On the other hand, one run was performed for each set of parameters of type β).

Table 4-I The parameters used for the experiments and the experimental data of wave velocity. All experiments were performed until 1,000,000 collisions were achieved in a 9,000 hard disk reacting system.

	Density $n\sigma^2$	Reaction heat ΔQ	Activation energy ε	Wave velocity[a)]	Mach number[a)]	Sound velocity[b)]
α	0.770	40.0	10.0	61.4	7.33	8.38
	0.385			20.1	7.00	2.87
	0.231			14.6	6.94	2.10
	0.116			12.1	7.08	1.71
β	0.385	40.0	10.0	20.0	6.97	2.87
			20.0	19.7	6.86	
		80.0	10.0	32.2	11.21	
			20.0	28.4	9.89	
		160.0	20.0	40.0	13.93	

a) For each set of parameters of type α), three runs were performed and the listed data of wave velocity and Mach numbers are the average values over the three runs. On the other hand, one run was performed for each of type β).

b) Sound velocities are evaluated for the upper stream region using eq. (4.3.16).

In Fig 4.1, the spatial distribution of the created B particles for one of the three runs of type α) $n\sigma^2 = 0.770$, $\varepsilon = 10.0$ and $\Delta Q = 40.0$ is shown. These parameters are the same as those used in chapter III. In this figure, we can see a B-rich region spreading from the left to the right. This region corresponds to the burnt gas, and the boundary of this region is regarded as a reaction wave front (combustion wave). In Fig 4.2, the time dependence of the position of the reaction wave front in Fig 4.1 is shown. Here, the position of the wave front is determined from the spatial distribution of B particles shown in Fig 4.1, errors being at most $\sim 10\sigma$. We found that the reaction wave propagates with a constant velocity. The averaged velocity of three runs for this set of parameters is 61.4. In order to know the real physical magnitude of this propagation velocity, it is convenient to normalize the velocity using the sound velocity for the upper stream region. As the upper stream region in our experiments is equivalent to the equilibrium state of the non-reactive hard disk system of temperature T_0 (note that no reactive collision takes place in this region), we can estimate the sound velocity with use of a thermodynamic relation (see next section). With this sound velocity, we can see the above mentioned propagation velocity of the reaction wave 61.4 corresponds to Mach 7.33. Therefore, the propagation of the reaction wave is a supersonic phenomenon. The other experiments for the parameters listed in Table 4-I also showed steady propagation of the reaction wave with a supersonic velocity. The experimental values of the propagation velocity and the Mach

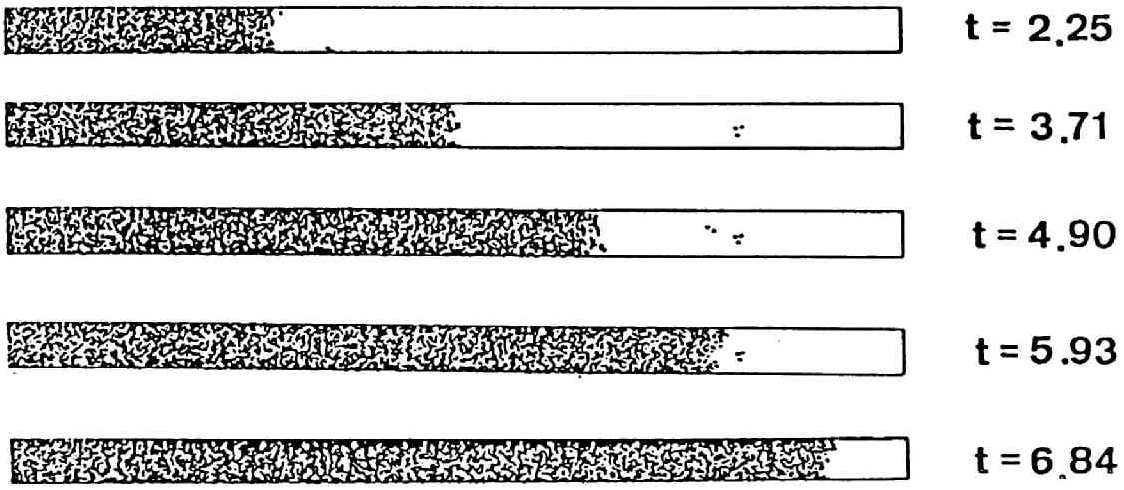

Fig. 4.1

An example of the time variation of spatial distribution of the created B particles is shown. We can see a one-dimensional propagation of the reaction wave from the left to the right. In this experiment, parameters are selected as $n\sigma^2 = 0.770$, $\varepsilon = 10.0$ and $\Delta Q = 40.0$.

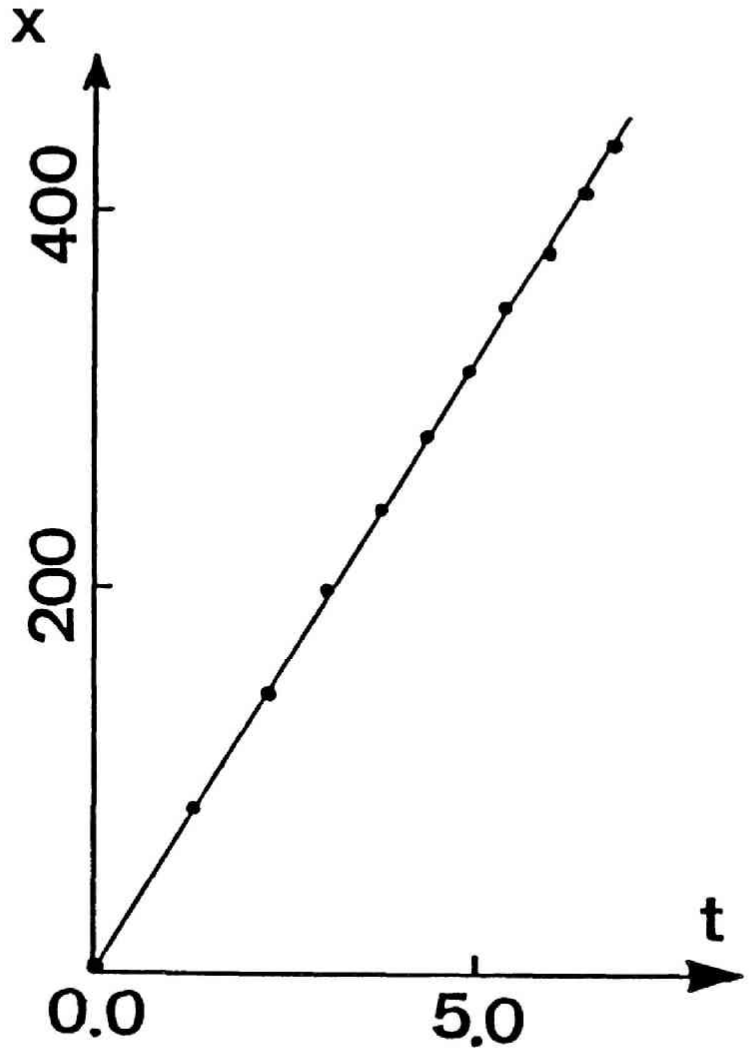

Fig. 4.2

Time dependence of the position of the wave front presented in Fig. 4.1 is shown.

number of the reaction wave are shown in Table 4-I. It is found that the wave velocity is sensitive to the density $n\sigma^2$ and the reaction heat ΔQ, but less sensitive to the activation energy ε. This suggests that the activation energy is irrelevant to the propagation mechanism of the wave.

Next, we calculate the thermodynamic structure of this reaction wave. For hard disk system, pressure is usually calculated using the virial theorem. Since the numbers of particles of respective species are not constant but fluctuate, the ensemble average in the virial theorem should be regarded as the average in the grand canonical ensemble;

$$\frac{PV}{Nk_BT} = 1 - \frac{1}{2Nk_BT} \left\langle \sum_i \vec{r}_i \cdot \frac{\partial \Phi}{\partial \vec{r}_i} \right\rangle . \qquad (4.2.2)$$

Here, Φ is the total inter-particle potential, $\vec{r}_i$ is the position of the i-th particle and $\langle\ \rangle$ denotes the average in grand canonical ensemble. Using the fact that there are no inter-particle forces during the interval between collisions, we can rewrite eq. (4.2.2) as follows;

$$\frac{PV}{Nk_BT} = 1 + \frac{1}{2Nk_BTt} \sum (\vec{r}_i - \vec{r}_j) \cdot \Delta\vec{p}_i \quad , \qquad (4.2.3)$$

where i and j are the indices of the colliding pair of each collision, $\Delta\vec{p}_i$ is the change in momentum of particle i on the collision and the summation is taken over all the collisions which have occurred in the objective region of volume V during

the time interval of t. We calculate the pressure of the reacting system using eq. (4.2.3).

In Fig. 4.3, the profiles of a) pressure, b) temperature and c) the number of net forward reaction ((forward) - (reverse)) per unit area per unit time are shown for the reaction wave presented in Fig 4.1. All quantities are measured on a coordinate system moving with the wave front, the origin of which corresponds to the reaction wave front. The plotted points are derived as follows; The system is divided into many sections along the x-direction in the above-mentioned coordinate system. The width of each section, say Δx, is taken to be $\Delta x = L_x / 300.0$. Therefore, each section contains about 30 particles, over which pressure, temperature and the number of reactions are averaged. Each value of temperature is evaluated using the root mean square of the velocities of particles in each section at t = 3.03. On the other hand, each values of pressure and the number of reactions are measured from about 300 collision data experienced by the particles in each section during a time interval $3.03 \leq t \leq 3.71$. We see a steep increase of pressure and temperature at the wave front. This structure is characteristic of a shock wave. Therefore, we see that the reaction wave is accompanied by a shock compression in front of it.

It is known that there are two types of combustion wave, one is called a deflagration and the other a detonation.[3,4] A deflagration is the usual combustion wave which propagates with a subsonic velocity. On the other hand, a detonation is a supersonic combustion wave which has a preceding shock wave.

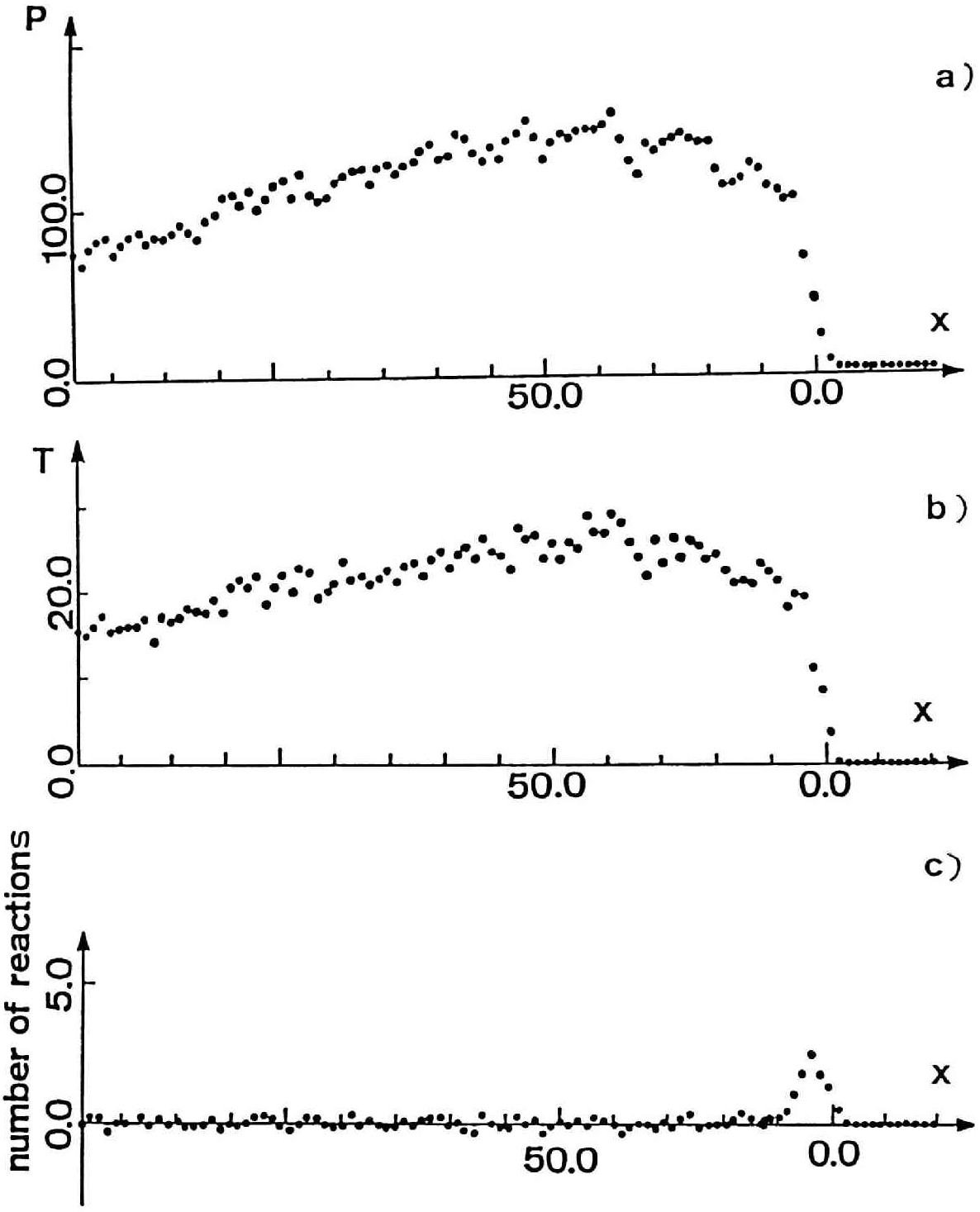

Fig. 4.3

The profiles of the wave front of Fig. 4.1 are shown; a) pressure, b) temperature and c) the number of net forward reaction per unit area per unit time.

Therefore, the reaction wave of our MD experiment has the characteristics of a detonation.

§ 4.3 Hydrodynamic Theory

In this section, we derive the stable detonation velocity for our hard disk reaction system, following the hydrodynamic theory.[4)]

Now we consider a steady one-dimensional propagation of a combustion wave. The basic equations are mass, momentum and energy conservation equations and they are given in the co-ordinate system moving with the wave as follows;

$$\rho_1 u_1 = \rho_2 u_2 \quad , \tag{4.3.1}$$

$$P_1 + \rho_1 u_1^2 = P_2 + \rho_2 u_2^2 , \tag{4.3.2}$$

$$h_1 + \frac{1}{2} u_1^2 = h_2 + \frac{1}{2} u_2^2 \quad . \tag{4.3.3}$$

Here, ρ is the mass density , u the flow velocity of the fluid, P the pressure, h the enthalpy per unit mass defined as $h = e + PV$ and e is the internal energy per unit mass. Subscripts 1 and 2 indicate the upper stream (reactant) and the down stream (burnt) state, respectively. From eqs. (4.3.1) and (4.3.2), we can represent the wave velocity u_1 as

$$u_1^2 = -V_2^2 \frac{P_2-P_1}{V_2-V_1} \quad . \tag{4.3.4}$$

Here, $V = 1/\rho$ is the volume per unit mass. From eq. (4.3.4) we see that u_1, the wave velocity against the upper stream fluid, is proportional to the square root of the slope of a straight line, so-called Rayleigh line, connecting the two points (P_1,V_1) and (P_2,V_2) on the P-V plane. On the other hand, from eqs. (4.3.1)-(4.3.3) we obtain

$$h_2 - h_1 = \frac{1}{2}(P_2 - P_1)(V_2 + V_1) \quad , \tag{4.3.5}$$

which is called Rankine-Hugoniot equation. If we consider P_2 and V_2 in eq. (4.3.5) as unknown variables, this equation gives the allowed point for state 2 on the P-V plane, provided the initial pressure P_1 and volume V_1.

Now we evaluate eq. (4.3.5) for our hard disk system. As there is no inter-particle potential energy in hard disk system, the internal energy e is composed of the thermal energy Nk_BT and the chemical energy e_c:

$$e = Nk_BT + e_c \quad . \tag{4.3.6}$$

Here, N is the total number of particles per unit mass. If we denote the released chemical energy during the change from state 1 to state 2 as q, we obtain

$$e_{c1} = e_{c2} + q \ . \qquad (4.3.7)$$

Substituting eqs. (4.3.6) and (4.3.7) into eq. (4.3.5), we obtain

$$\frac{1}{2}\,(P_2 - P_1)(V_2 + V_1) = Nk_B(T_2 - T_1) + (P_2V_2 - P_1V_1) - q \ . \qquad (4.3.8)$$

When the system is composed of same numbers of A's and S's in state 1, the equilibrium number of created B particles in state 2, which is denoted as N_B, is given by

$$N_B = \frac{N}{2\ (\ 1 + \exp(\ -\Delta Q/k_BT_2))} \ , \qquad (4.3.9)$$

which is immediately derived from the Boltzmann factor. We can evaluate q using eq. (4.3.9) as

$$q = N_B\Delta Q \ . \qquad (4.3.10)$$

Therefore, with use of eqs. (4.3.9) and (4.3.10), the Rankine-Hugoniot equation (4.3.8) for our hard disk reacting system is given by

$$(P_2 + P_1)(V_2 - V_1) + 2Nk_B(T_2 - T_1) = \frac{N\Delta Q}{1 + \exp(\ -\ \Delta Q/k_BT_2)} \ . \qquad (4.3.11)$$

In eq. (4.3.11), temperature T can be expressed by pressure P and volume V with the use of the Pade approximation of the equation of state of the hard disk system[57] both for state 1 and state 2. The validity of applying this equation of state of non-reactive hard disk system to state 2, which is the equilibrium state of a reactive hard disk system, is discussed in the next section. In this way, we can draw the Rankine-Hugoniot curve on the P-V plane.

It is known that the stable detonation wave is represented by the point at which the Rayleigh line contacts tangentially with the Rankine-Hugoniot curve. This point is called as upper Chapman-Jouguet point (upper CJ point).[4]

If the reaction heat ΔQ is much larger than $k_B T_1$, it can be shown that the stable detonation velocity evaluated at the upper CJ point is proportional to $(\Delta Q)^{1/2}$ with use of eq. (4.3.11) as follows. If we define $\tilde{P}$ as $\tilde{P} = P / \Delta Q$, then eq. (4.3.11) leads to

$$(\tilde{P}_2 + \tilde{P}_1)(V_2 - V_1) + 2Nk_B\left(\frac{T_2 - T_1}{\Delta Q}\right) = \frac{N}{1 + \exp(- \Delta Q/k_B T_2)} \cdot \tag{4.3.12}$$

If we use the equation of state

$$\frac{PV}{Nk_B T} = 1 + f\left(\frac{N}{V}\right) , \tag{4.3.13}$$

where f is a function of only density, and eliminate temperature in eq. (4.3.12), we obtain

$$(\tilde{P}_2 + \tilde{P}_1)(V_2 - V_1) + 2\left[\tilde{P}_2 V_2 (1 + f(\frac{N}{V_2}))^{-1} - \tilde{P}_1 V_1 (1 + f(\frac{N}{V_1}))^{-1} \right] = \frac{N}{1 + \exp(- N(1 + f(N/V_2))/\tilde{P}_2 V_2)} . \qquad (4.3.14)$$

As is seen from eq. (4.3.14), Rankine-Hugoniot curve is independent of ΔQ when it is drawn on the $\tilde{P}$-V plane. On the other hand, the Rayleigh line is a line connecting the two points $(\tilde{P}_1, V_1)$ and $(\tilde{P}_2, V_2)$ on the $\tilde{P}$-V plane. If we assume that $\Delta Q >> k_B T_1$, then we can put $\tilde{P}_1 \simeq 0$ while $\tilde{P}_2$ is finite. Therefore, the Rayleigh line on the $\tilde{P}$-V plane can approximately be regarded as a line connecting the two points $(\tilde{P}_2, V_2)$ and $(0, V_1)$ on the $\tilde{P}$-V plane. Then the Rayleigh line is also independent of ΔQ. As a result we see that the upper CJ point on the $\tilde{P}$-V plane is independent of ΔQ and the slope of the Rayleigh line which passes through the upper CJ point is also independent of ΔQ on the $\tilde{P}$-V plane. As is mentioned previously, since the detonation velocity is proportional to the square root of the slope of the Rayleigh line on the original P-V plane, the detonation velocity is proportional to $(\Delta Q)^{1/2}$.

Finally, we present an expression for the sound velocity in a hard disk system. The sound velocity c is obtained from the thermodynamic relation;

$$c^2 = \left[\frac{\partial P}{\partial \rho}\right]_S . \qquad (4.3.15)$$

As for the hard disk system, this relation leads to

$$c^2 = V^2\left[\frac{P}{R}\left[\frac{\partial P}{\partial T}\right]_V - \left[\frac{\partial P}{\partial V}\right]_T \right], \qquad (4.3.16)$$

where $R = k_B/m$ is the gas constant per unit mass. Together with the equation of state of the hard disk system,[57] we can evaluate the sound velocity from eq. (4.3.16), which are given in Table 4-I.

§ 4.4 Comparison between Experiment and Theory

We evaluated the upper CJ point and the stable detonation velocity from eqs. (4.3.4) and (4.3.11) for the values of $n\sigma^2$ and ΔQ, listed in Table 4-I α). As was mentioned in §. 4.3, we applied the equation of state for the non-reactive hard disk system[57] in order to evaluate the temperature in state 2. In order to check the validity of this equation of state for our reacting hard disk system, we performed different runs. From these runs (data from the 1,000,000 collisions in equilibrium state of 10,000 reacting hard disks), we confirmed that the equation of state is valid even for the equilibrium state of our reactive system within an accuracy of 1 %. So we can use the equation of state for state 2 as well as state 1. In Figs 4.4 and 4.5, we present the experimental (MD) and the theoretical (eqs. (4.3.4) and (4.3.11)) values of the wave velocities. Density dependence of the wave velocity is shown in Fig 4.4,

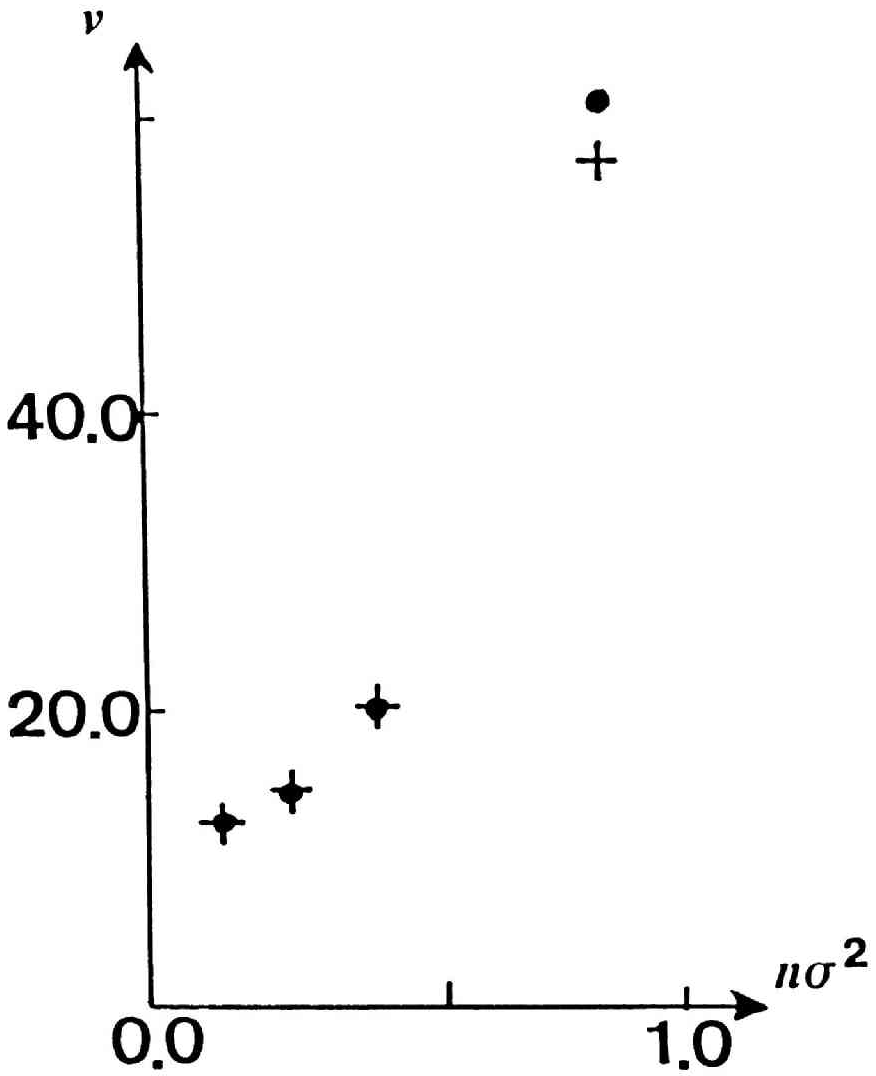

Fig. 4.4

Comparison between the theoretical values (cross) from eqs. (4.3.4) and (4.3.11) and the experimental values (solid circle) of the wave velocity is made for a variety of number density of particles $n\sigma^2$. Here, $\Delta Q = 40.0$ is kept constant.

while dependence on the reaction heat ΔQ is shown in Fig 4.5. As was theoretically demonstrated in § 4.3, the experimental wave velocity is seen to be proportional to $(\Delta Q)^{1/2}$. Dependence of the wave velocity on the activation energy ε was not noticeable (see Table 4-I). Agreement between the experimental values and the theoretical values is achieved within an accuracy of a few percent. From these results and the structure of the reaction wave mentioned in § 4.2, we can conclude that the reaction wave in our MD experiments is a detonation.

We also calculated the theoretical values of the thermodynamic variables in state 2 (downstream state), defined as the upper CJ point, from eqs. (4.3.4) and (4.3.11). On the other hand, the corresponding experimental values are calculated in the region enough backward of the wave front. In Table 4-II, both these theoretical values and the experimental values are shown. The agreement between them is not good. It is thought that this disagreement is caused by the elastic wall condition we imposed to the wall at $x = 0$, whereas the steady flow condition is assumed in the theory. From this disagreement and the agreement between the theoretical and experimental values of the wave velocity shown in Figs 4.4 and 4.5, we see that the wave velocity is insensitive to the state of the downstream region. That is, the wave velocity is mainly determined by the condition in the narrow region at the wave front. This is also confirmed by the fact that the wave velocity is proportional to $(\Delta Q)^{1/2}$. The quantity $(\Delta Q)^{1/2}$ is the corresponding velocity to the released reaction heat. Therefore the $(\Delta Q)^{1/2}$ dependence of the wave

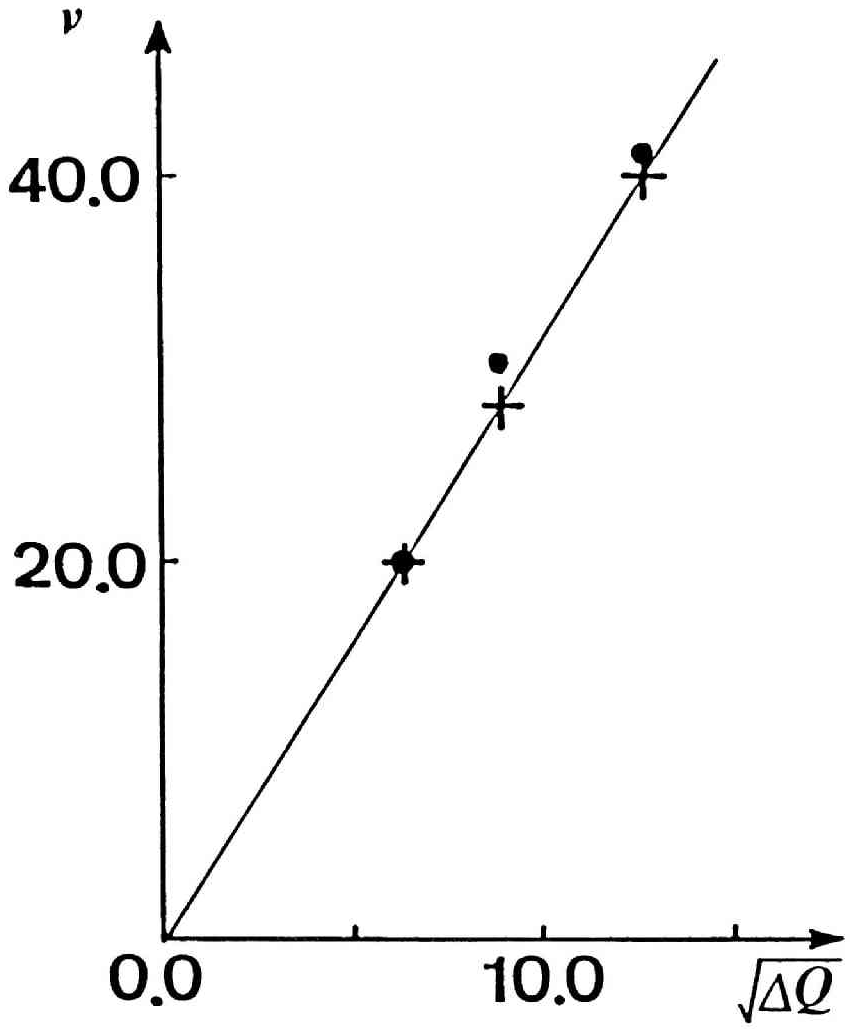

Fig. 4.5

Theoretical values (cross) and the experimental values (solid circle) of the wave velocity are shown for a variety of square root of the reaction heat $(\Delta Q)^{1/2}$. Here, $n\sigma^2 = 0.385$ is kept constant.

Table 4-II Comparison between the theoretical values and the experimental values of the thermodynamical variables of the downstream region. All experimental data are the averaged values over three runs of type α) in Table 4-I.

	Upper CJ point (Theoretical)			State 2 (Experimental)		
$n\sigma^2$ [a]	V/V_1 [b]	P/P_1 [b]	T	V/V_1 [b]	P/P_1 [b]	T
0.770	0.93	37.36	26.70	1.04	13.55	15.59
0.385	0.82	37.12	24.80	1.10	13.14	15.52
0.231	0.76	37.60	24.64	1.12	13.60	15.87
0.116	0.71	37.53	24.49	1.23	12.23	15.51

a) The other parameters ΔQ, ε and T_1 are kept constant at 40.0, 10.0 and 1.0, respectively.

b) The volume and the pressure are normalized by the corresponding values in the state 1 (upper stream region).

velocity indicates that the momentum flow is steadily maintained by the successive reactive collisions of the particles at the wave front.

§ 4.5 Concluding Remarks

In the preceding sections, we found that, in some respects, our reactive hard disk system can reproduce a detonation both qualitatively and quantitatively. Therefore, we can conclude that a detonation, which is a highly nonequilibrium phenomena, can be realized by only three properties which our model maintains; translational motion, change of species and release of heat. The most remarkable difference between the detonation of our experiments and the real one is the position of the reaction zone. As is shown in Fig 4.3, the reaction zone of the experimental detonation locates immediately after the wave front. While it is known that the reaction zone of the real detonation locates somewhat backward of the front[4]. This is caused by the relaxation of the translational energy, which the molecule gains through the passage of the shock wave, to the internal mode of the molecule which induces the reaction. As our hard disk system does not have these internal degrees of freedom, the excess translational energy from the shock compression immediately raises up the reaction. So the location of the reaction zone coincides with the wave front. Recently, Tsai and Trevino[31] studied a detonation in a diatomic molecular crystal using MD

method. The structure of the detonation of their experiment is similar to our results. Only difference is that the reaction zone in their experiment locates backward of the shock front, which originates from the fact that their model molecule has the internal degrees of freedom. Therefore, the characteristic structure of our detonation is due to the lack of the internal degrees of freedom of the hard disk system. Taking these internal degrees of freedom into account in our model will be discussed in chapter VII.

We also found that the driving mechanism lies in the narrow region at the wave front. The thickness of this region is the same order as the mean free path. In such a microscopic region, discreteness of the fluid is by no means negligible. Further analyses on the dynamics in the scale of the inter-particle distance are presented in the next chapter.

CHAPTER V

DETONATION WAVE: ENERGY RELAXATION PROCESSES AT THE WAVE FRONT

§ 5.1 Introduction

The elucidation of many-body correlation is one of the central problems in condensed matter physics. To study this problem for classical particle system directly, the molecular dynamics (MD) method has been playing an important role.[6-11)]

In the previous chapter (chapter IV) with the MD method, we studied a reaction wave propagation in a hard disk system which undergoes an exothermic reaction. We found that the generated reaction wave corresponds to a detonation. A detonation is a supersonic combustion wave which is accompanied by a shock compression in front of it, and the thickness of the shock front is of the order of the mean free path of the particles. Therefore, information on the molecular level microscopic dynamics of the particles at the detonation wave front is required in order to understand the mechanism of the propagation of the detonation. We found that the propagation velocity of the detonation is in good agreement with the theoretical value of the stable detonation velocity obtained with a hydrodynamic theory. In this chapter, we investigate the energy relaxation processes

at the detonation wave front. Especially, we are interested in the effects of the many-body correlation among particles on the propagation mechanism of the detonation.

In the next section we summarize the model used for the MD experiments. In § 5.3 the dependence of the detonation velocity on the molar fraction of each species is studied and compared with a hydrodynamic theory. The energy relaxation processes at the detonation wave front are examined in detail and the results are shown in § 5.4. Finally in § 5.5 we make some remarks.

§ 5.2 Summary of the Model for MD Experiments

The model reaction system used in this chapter is the same as that used in the previous chapter (chapter IV). We prepare a hard disk system, in which each disk has an identical mass m and a diameter σ. We introduce an exothermic isomerization reaction, which is expressed as

$$A + S \underset{\leftarrow}{\overset{\rightarrow}{}} B + S + \Delta Q \quad , \qquad (5.2.1)$$

$$(\Delta Q \geq 0)$$

into the hard disk system.

In order to observe the detonation propagation phenomena, we set 9,000 hard disks in a rectangular box whose side length L_x and L_y are in the ratio 20 : 1. We take the x-coordinate along the longer side L_x and y-coordinate along the shorter side L_y,

respectively. A periodic boundary condition is imposed only for the y-direction and the walls on the shorter sides are assumed to be elastic. After realizing an equilibrium state of the non-reactive hard disk system at temperature T_0, we assign species A or S to each disk spatially randomly according to an uniform distribution. Then, the particles of which x-coordinates are in the region $0 \leq x \leq L_x/50$ are heated by multiplying their velocities by a factor of 5.0 in order to initiate a detonation. The A particles in this region begin to make reactions and turn into B particles by releasing the reaction heat. The released reaction heat induces next reactive collisions and in this way the reactive region propagates in the x-direction, that is, a detonation propagates.

In chapter IV, each molar fraction of species A and S in the initial state was fixed to be 0.5, that is, the number of particles of species A was equal to that of species S. In this chapter, we change these molar fractions in order to investigate the effects of composition on the detonation propagation mechanism.

Hereafter we present the results of computations by dimensionless quantities using the units of mass m, length σ, time $(m\sigma^2/k_BT_0)^{1/2}$ and energy k_BT_0, except for § 5.4 and the Appendices where the derivation of expressions is done with the quantities which are not normalized for the convenience of the readers.

§ 5.3 Detonation Velocity : MD Experiment and Theory

We performed a series of MD runs with the parameters listed in Table 5-I. In the table, the quantity c_R is the molar fraction of the total reactive species A and B, which is invariant through the reaction process. Therefore, $1 - c_R$ means the molar fraction of species S. The parameters $n\sigma^2$, ΔQ and ε indicate the dimensionless number density of hard disks, reaction heat and the activation energy of the forward reaction, respectively. The case $n\sigma^2 = 0.770$ corresponds to a high density fluid phase of the hard disk system, while the case $n\sigma^2 = 0.116$ to a low density fluid phase.

For each run we observed that a B-rich region, which corresponds to the burnt gas region, spreads along the x-direction. The boundary of the B-rich region corresponds to the detonation wave front. As an example, in Fig. 5.1 we show the time dependence of the position of wave front, which is determined from the spatial distribution of created B particles, for the case of $n\sigma^2 = 0.770$ and $c_R = 0.75$. The straight line in this figure is drawn with the least square method. The obtained detonation velocities for various c_R values and densities are also shown in Table 5-I.

Figure 5.2 shows the detonation velocities as a function of c_R, where the theoretical values obtained by a hydrodynamic consideration (see Appendix A) are also shown for comparison. To derive the theoretical values, we assumed that the down stream

Table 5-I The parameters used in the MD experiments and the MD results of the detonation velocity.

In each case, the parameters ε and ΔQ are 10.0 and 40.0, respectively, and one computation run was performed for the each set of parameters.

$n\sigma^2$	c_R	Detonation velocity (MD)
0.770	0.25	47.3
	0.50	64.2
	0.75	62.6
	0.90	51.3
0.116	0.25	9.0
	0.50	12.1
	0.75	13.7
	0.90	14.0

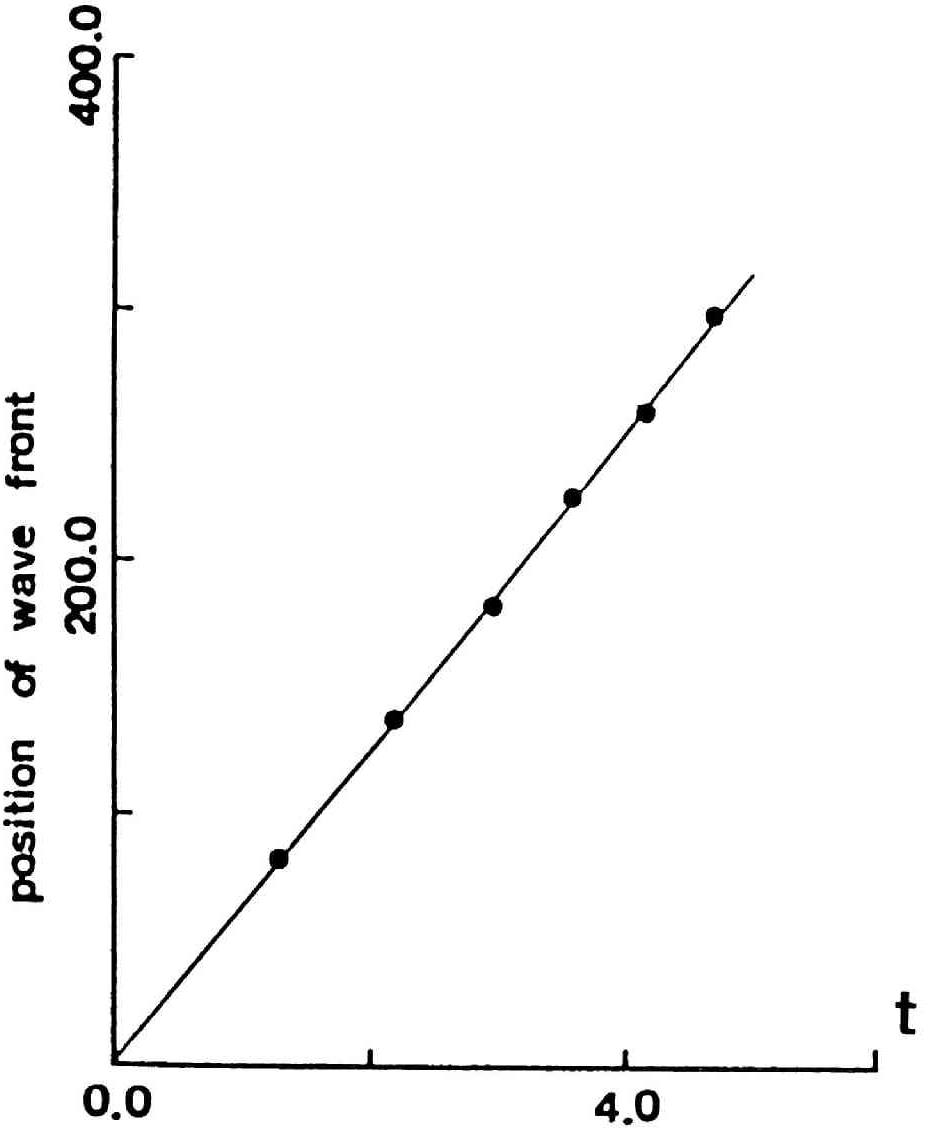

Fig. 5.1

The time dependence of the position of the detonation wave front is presented for the case $n\sigma^2 = 0.770$ and $c_R = 0.75$. Here, the time and position are non-dimensionalized with use of the units of length σ and time $(m\sigma^2/k_B T_0)^{1/2}$. The straight line in the figure is determined by a least square method with which the detonation velocity is evaluated.

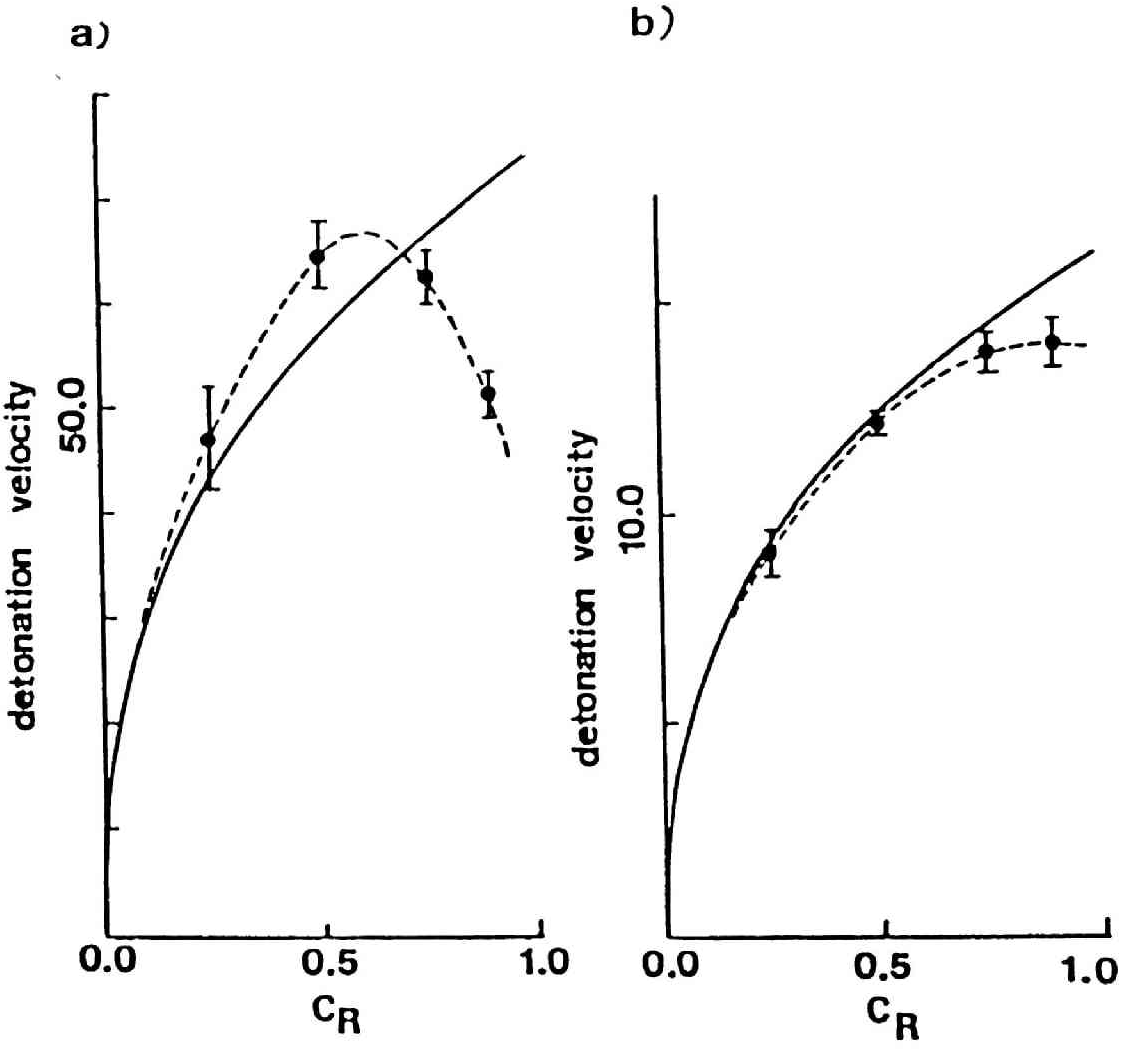

Fig. 5.2

Dependence of the dimensionless detonation velocity on the molar fraction of reactive species (A + B) is shown for (a) $n\sigma^2 = 0.770$ and (b) $n\sigma^2 = 0.116$. Solid circles indicate the MD results and the solid curve shows the theoretical values obtained from eq. (A.3). The probability that the true value lies within the error bar is 95%.

region of the detonation is in chemical as well as thermal equilibrium.

From Fig. 5.2 we see that the agreement between the results of the MD and the theory is good except for the high density and large c_R region, where the MD results are systematically smaller than the theoretical values. We expect that in the region mentioned above the equilibrium assumption used in the hydrodynamic calculation is not valid for the down stream region. In the high density and large c_R region, the number of A particles are much more abundant than that of S particles, so there exist considerable numbers of clusters composed of only A and B particles. For the A particles inner in such clusters, there is no neighboring S particle and they have less possibility to experience reactive collisions with S particles. As a result the A particle is considered to be trapped in a cage. We can imagine that such cage effect works to suppress reactive collisions to occur and reduces the detonation velocity compared with the theoretical value. This point is discussed in the next section.

§ 5.4 Relaxation of Energy at the Wave Front

5.4.1 Methods of calculation and the results

In order to clarify the cage effect suggested in the preceding section, we investigate the energy relaxation processes at the detonation wave front.

As is mentioned in § 5.3, the position of the wave front $x(t)$ can be fitted to a linear function of time as $x(t) = vt + x_0$. We determined these two parameters v and x_0 with the use of the least square method. Using this expression, we evaluate the time when the wave front passes over the i-th particle and we denote it as $t_i^{(0)}$. Now, we define an ensemble average of any quantity $Q_i(t)$ associated with the i-th particle, such as the particle velocity, as follows:

$$\langle Q(\tau) \rangle \equiv \frac{1}{N} \sum_{i=1}^{N} Q_i(t-t_i^{(0)}), \qquad (5.4.1)$$

where N is the number of sample particles and τ is defined as $\tau \equiv t-t_i^{(0)}$ for the i-th particle. The quantities $t_i^{(0)}$'s are constants and independent of the ensemble average. By this definition of $\langle Q(\tau) \rangle$ we can investigate how $\langle Q(\tau) \rangle$ changes before and after the passage of the wave front. Hereafter, we use the notation t instead of τ.

In Fig. 5.3 the time evolution of various physical quantities is presented for the case $n\sigma^2 = 0.770$ and $c_R = 0.75$.

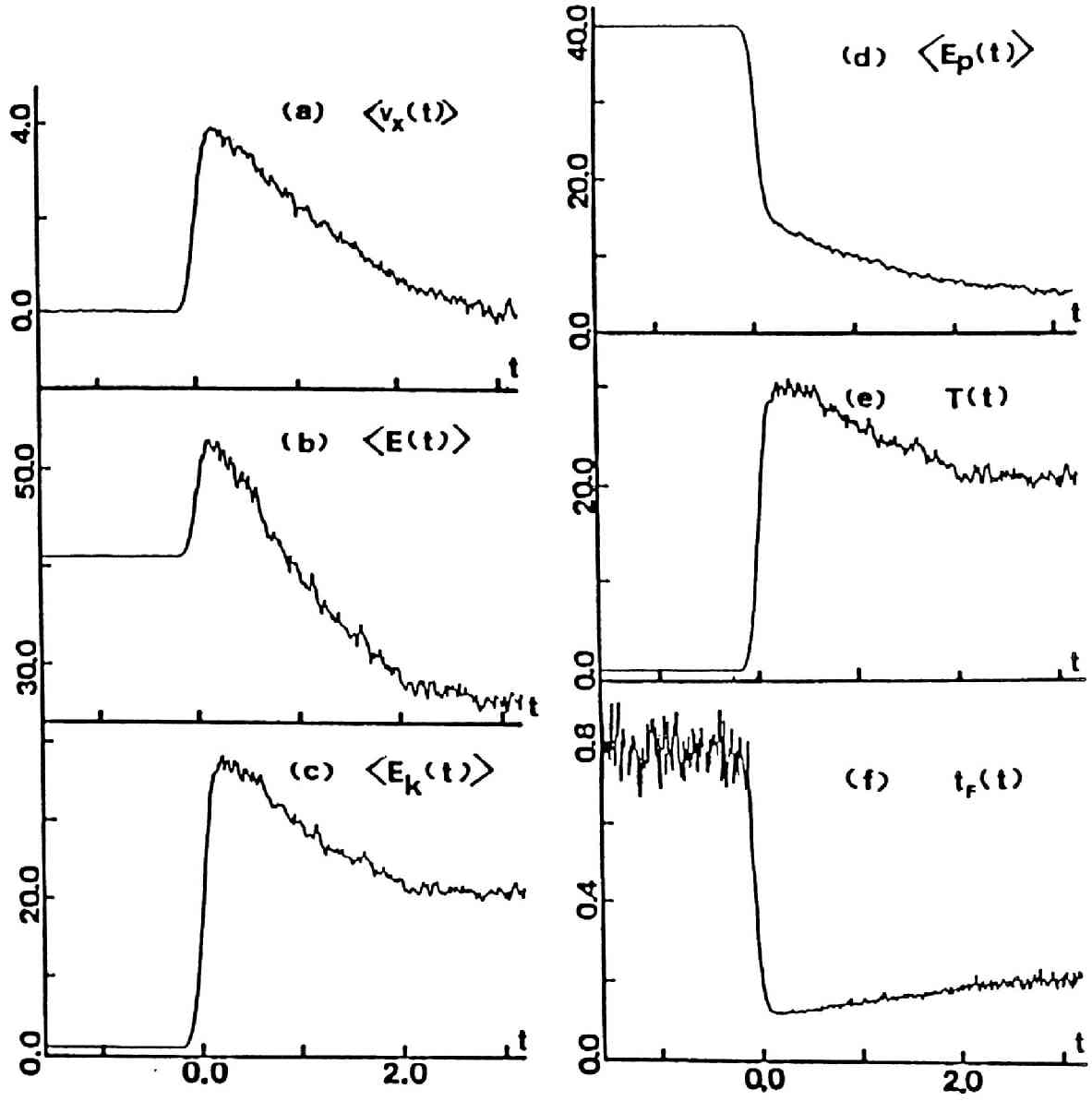

Fig. 5.3

Time evolutions of averaged dynamical quantities of particles; (a) x-component of the particle velocity, (b) total energy per particle, (c) kinetic energy per particle, (d) chemical energy per particle, (e) temperature (random part of the kinetic energy) and (f) mean free time, are shown for the case $n\sigma^2 = 0.770$ and $c_R = 0.75$. The time origin corresponds to the time when the detonation wave front determined by the straight line in Fig. 5.1 passes through the particle. Here all quantities are dimensionless.

The ensemble average was taken over all the particles of which species are A in the initial state. Each figure shows the evolution of (a) x-component of the particle velocity $\langle v_x(t) \rangle$, (b) total energy (kinetic energy plus chemical energy) per particle $\langle E_T(t) \rangle$, (c) kinetic energy per particle $\langle E_K(t) \rangle$, (d) chemical energy per particle $\langle E_P(t) \rangle$, (e) temperature T(t) and (f) mean free time $t_F(t)$, all of which are presented in dimensionless values. Here, kinetic energy is calculated from the mean square velocity of particles and includes the components of the systematic flow which are expressed by the x and y-components of the mean velocity. On the other hand, contributions of these systematic flow are not included in the temperature. As a chemical energy the value ΔQ is assigned to species A and the value 0 to species B. So the quantity $\langle E_P(t) \rangle$ is directly proportional to the number of the surviving fraction of A particles at time t. Mean free time $t_F(t)$ is calculated by counting the number of collisions of each particle occurred in a small time interval at time t.

A rapid movement of the particles along the x-direction due to the shock compression is clearly seen in Fig. 5.3(a). Due to this compression and the release of the reaction heat, the total energy (Fig. 5.3(b)) as well as temperature (Fig. 5.3(e)) increases abruptly and then the total energy begins to decrease which is due to the relaxation of both the kinetic and the chemical energies as shown in Figs. 5.3(c) and 5.3(d). The quantities $\langle v_x(t) \rangle$, $\langle E(t) \rangle$, $\langle E_K(t) \rangle$ and T(t) make changes simultaneously in a step-wise manner. The $\langle E_P(t) \rangle$ decays due

to the loss of A particles through reactive collisions $A + S \rightarrow B + S$. We see that the time dependence of $\langle E_P(t) \rangle$ is composed of two time regions, one is a rapid decay in the early stage and the other a relatively slow decay in the late stage. Crossover from the first rapid region (region I) to the latter slow region (region II) occurs at the time when $\langle v_x(t) \rangle$ and $\langle E(t) \rangle$ take their maximum values (for example, compare Figs. 5.3(a) and 5.3(d)).

To find the decaying rate in these two regions, we present semi-log plots of $\langle E_P(t) \rangle$ in Fig. 5.4 for (a) $n\sigma^2 = 0.770$ and (b) $n\sigma^2 = 0.116$. We see that two linear regions exist, which suggests an exponential decay of the form

$$\langle E_P(t) \rangle \propto \exp(- t / \tau), \qquad (5.4.2)$$

where τ is a relaxation time. The relaxation times τ_I and τ_{II} for the respective two time regions are derived with use of least square method and shown in Figs. 5.5 and 5.6 with solid circles for (a) region I and (b) region II. Compared with the mean free time $t_F(t)$, the relaxation times τ_I and τ_{II} are of the order of $10t_F$ and $100t_F$, respectively.

5.4.2 Decay process in region I

Relaxation processes in region I can mainly be explained by a simple non-correlated collision model. Consider an A particle

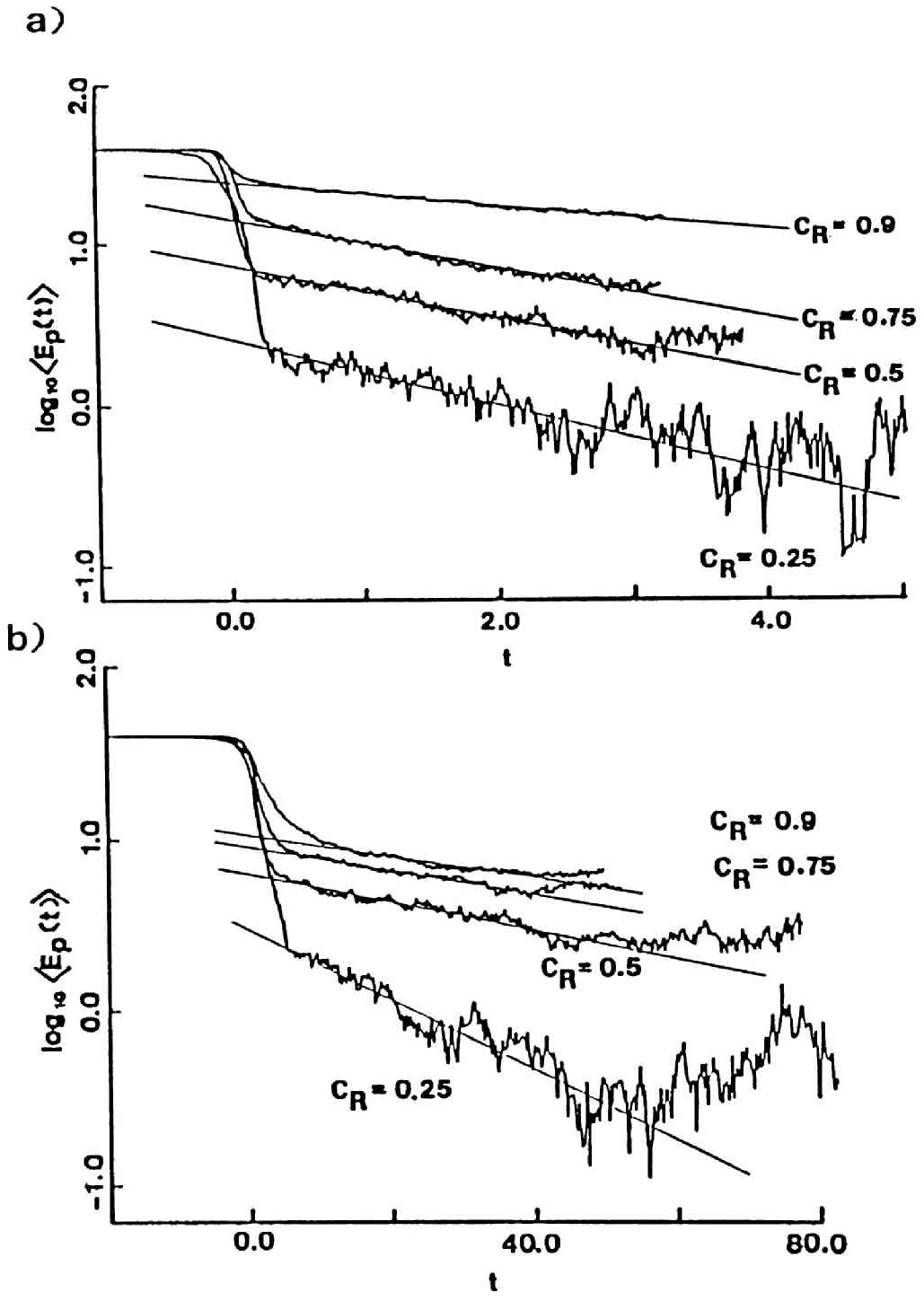

Fig. 5.4

Relaxation processes of the chemical energy of species A are shown for (a) $n\sigma^2 = 0.770$ and (b) $n\sigma^2 = 0.116$. Two kinds of exponential relaxation processes are observed. The straight lines are determined by least square method for region II. Here chemical energy and time are dimensionless.

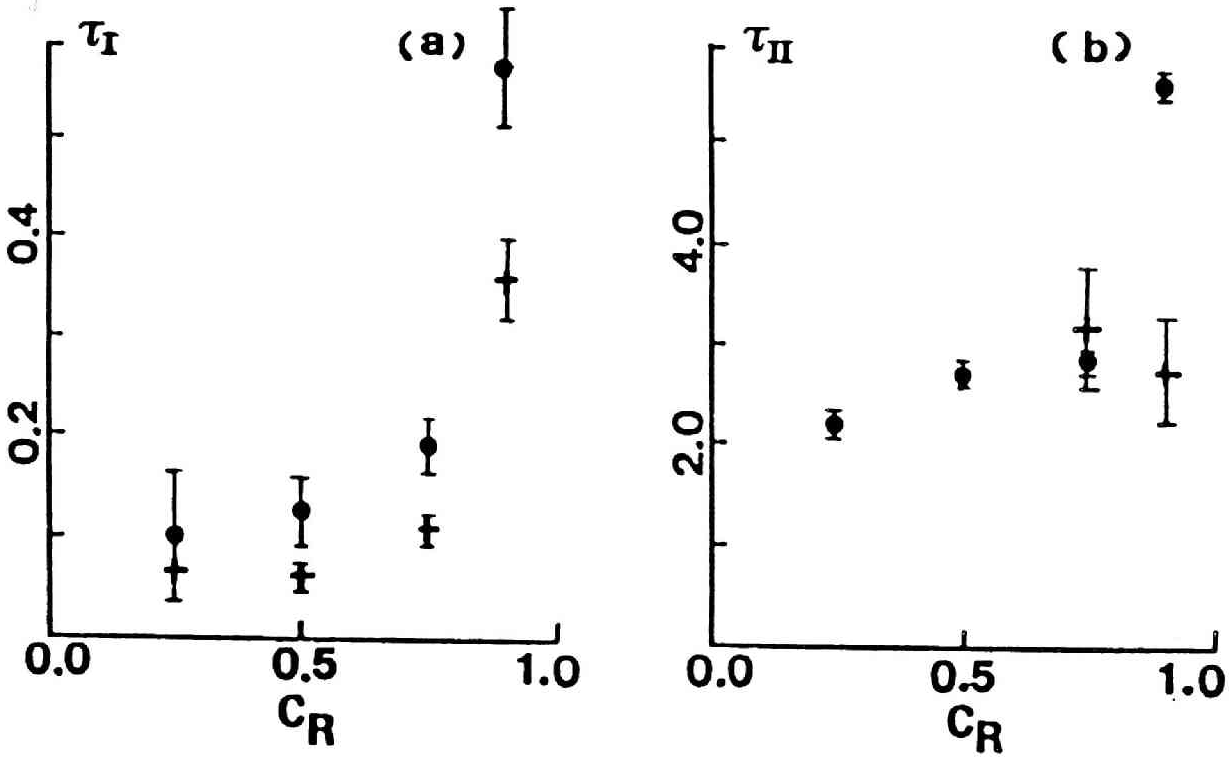

Fig. 5.5

The experimental (MD) values of the relaxation times τ_I and τ_{II} (dimensionless) for the case $n\sigma^2 = 0.770$ are shown for (a) region I and (b) region II with solid circles. In Fig. 5.5(a) the theoretical values, which are evaluated with eq. (5.4.5), are also shown with crosses. In Fig. 5.5(b) the relaxation times calculated from the decay processes of the mean cluster size of surviving A particles are shown with crosses for $c_R = 0.75$ and 0.9.

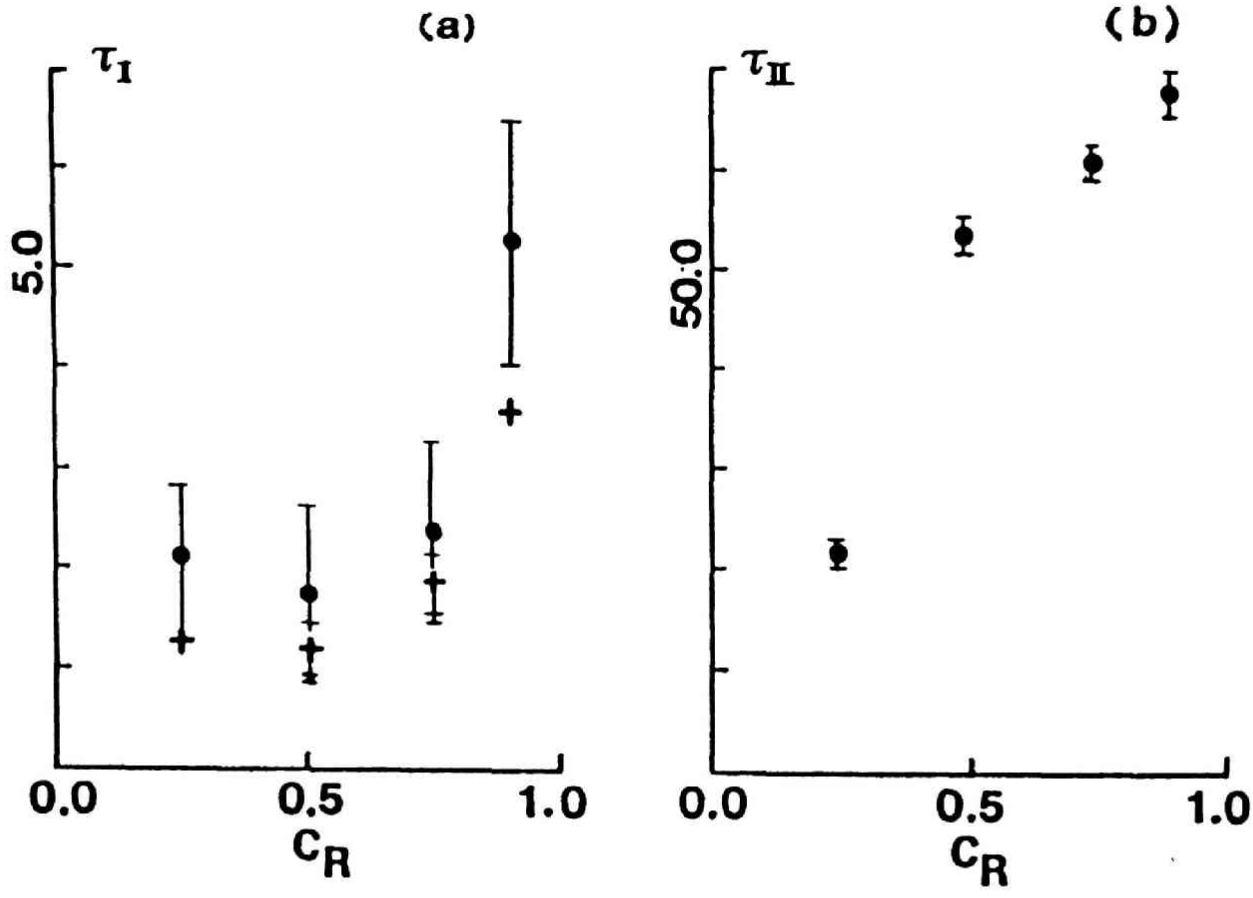

Fig. 5.6

The same as Fig. 5.5 for the case $n\sigma^2 = 0.116$.

at time $t = t_0$ ($t_0 < 0$). This A particle experiences $t_F^{-1}(t)$ collisions per unit time at time t. If the collisions have no correlation, one collision may be between non-reactive type pair (A + A or A + B) at the rate of c_R or reactive-type (A + S) at the rate $1 - c_R$. When the collision is a reactive-type, a reaction takes place at the rate

$$P_R(t) = \int_0^1 \exp\left(- \frac{1}{1-x^2} \frac{\varepsilon}{k_B T(t)} \right) dx \ , \qquad (5.4.3)$$

which is the probability that the head-on collision component of the relative kinetic energy at a collision exceeds the activation energy ε under temperature T(t) (see Appendix B). Here, we assumed that the system is in thermal equilibrium. Therefore, the probability that an A particle survives after a collision is expressed as

$$P(t) = c_R + (1 - c_R)(1 - P_R(t)) \ . \qquad (5.4.4)$$

As the quantity $< E_P(t) >$ is proportional to the fraction of surviving A particles, we obtain the next relation:

$$< E_P(t) > = \Delta Q \prod_{\{t_i\}} P(t_i), \qquad (5.4.5)$$

where the multiplication is taken over the sequence of successive collision times $\{t_i\}$. Using the MD data of T(t) and $t_F(t)$, we calculated $< E_P(t) >$ from eqs. (5.4.3)-(5.4.5) and the results

are shown in Fig. 5.7 with the fine curve for the case $n\sigma^2 = 0.770$ and $c_R = 0.75$ along with the MD data shown with the bold curve, which is the same as that shown in Fig. 5.4(a). Here as the time sequence (t_i) in eq. (5.4.5) we adopt a collision time sequence of idealized collisions of a particle which experiences successive collisions in which each time interval of collisions equals to the MD results of the mean free time $t_F(t)$. The agreement between the MD data and the theoretical results (eq. (5.4.5)) is fairly good for region I. From the theoretical curves thus obtained for all the cases in Table 5-I, we evaluated the theoretical values of τ_I which are shown in Figs. 5.5(a) and 5.6(a) with crosses. We see that the experimental relaxation times are fairly well reproduced by the theory. This indicates that the decay process in the region I is mainly determined by the successive non-correlated reactive collisions.

5.4.3 Decay process in region II

Now we look for the mechanism of region II. One of the important factors to be considered is the relaxation of temperature. As is shown in Fig. 5.3(e), after the temperature raises and takes its maximum value, it begins to decay slowly compared to the abrupt increase. This process is mainly caused by the decrease of density which has been raised by the shock compression. If we assume that the system is always in equilibrium at temperature T(t) in region II, the number of A

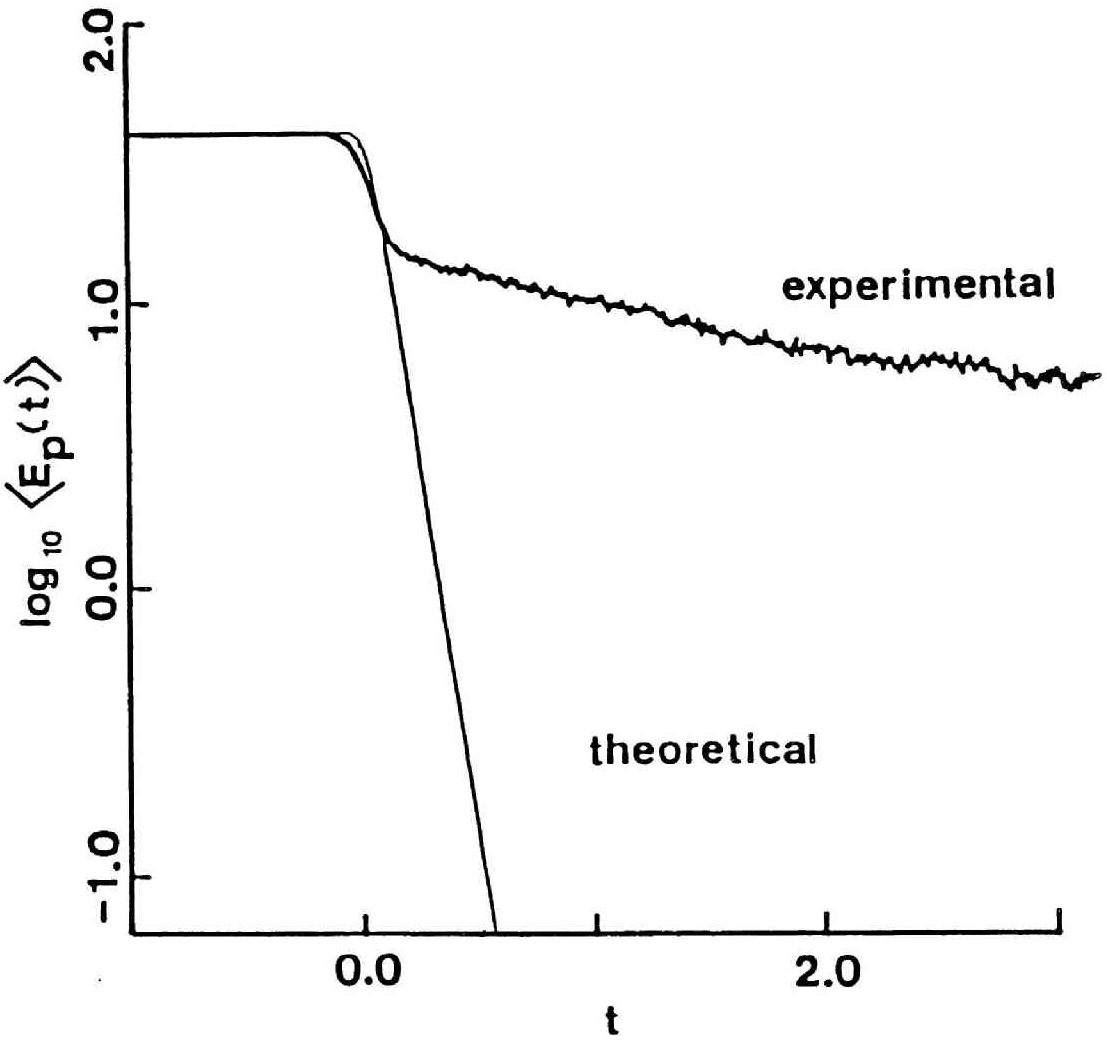

Fig. 5.7

The theoretical (eq. (5.4.5)) relaxation processes of the chemical energy is compared with the MD result. It is seen that eq. (5.4.5) well describes the behavior of the relaxation in region I.

particles per unit mass, N_A, becomes a function of T and is expressed as (see eq. (A.2))

$$N_A = c_R N \exp(-\Delta Q/k_B T) / \{ 1 + \exp(-\Delta Q/k_B T)\} , \quad (5.4.6)$$

and the chemical energy per particle is given by

$$\langle E_P(t) \rangle = \Delta Q \, N_A/c_R N , \quad (5.4.7)$$

where N is the total number of particles per unit mass. We calculated the expected values of $\langle E_P(t) \rangle$ in region II, assuming the system to be in equilibrium with temperature T(t), using eq. (5.4.7) with the data of T(t). The results are shown in Fig. 5.8 for the high density case ($n\sigma^2 = 0.770$). For small c_R, MD data and the data obtained by eq. (5.4.7) are in good agreement (Figs. 5.8(a) and (b)). For large c_R values, however, the decay process of $\langle E_P(t) \rangle$ can not fully be explained by the relaxation of temperature. On the other hand, in the low density case ($n\sigma^2 = 0.116$) we confirmed for all values of c_R used in the runs that the decay of $\langle E_P(t) \rangle$ is completely explained by the temperature relaxation. Therefore, the region in which eq. (5.4.7) cannot reproduce the behavior of relaxation is limited to the high density and large c_R region. As was noticed in § 5.3, such a region corresponds to the region where the MD and the theoretical detonation velocities are not in agreement. We expect that the cage effect becomes more important in such a region. As is suggested in § 5.3, a cluster composed

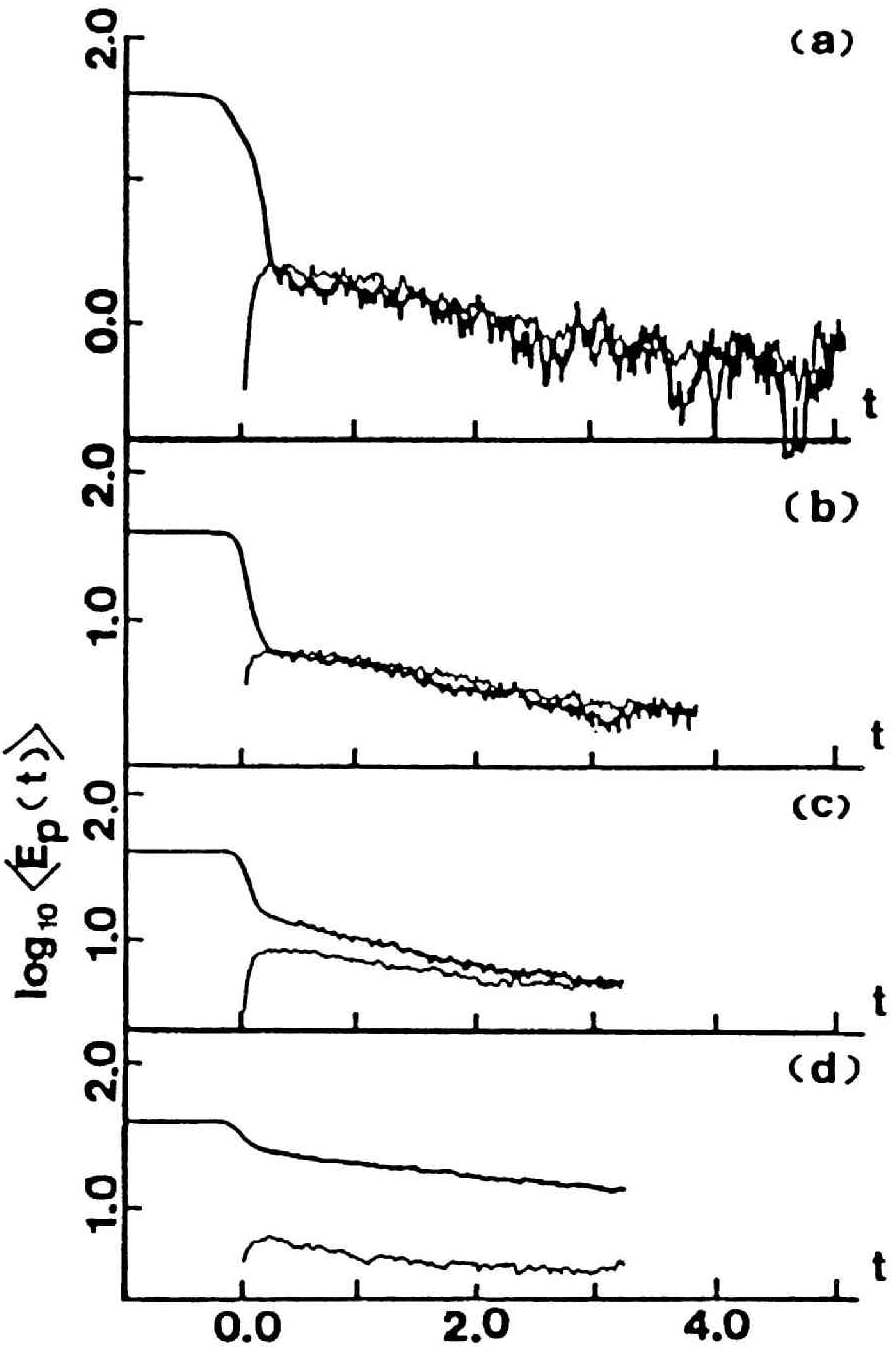

Fig. 5.8

Comparison between the experimental relaxation of $\langle E_P(t) \rangle$ (bold curve) and that obtained with an equilibrium assumption, eq. (5.4.7) (fine curve), is made for the high density case $n\sigma^2 = 0.770$. The parameter c_R is (a) 0.25, (b) 0.50, (c) 0.75 and (d) 0.90, respectively.

of only A and B particles plays the role of a cage which prevents the inner A particles from making reactive collisions (see Fig. 5.9). If this clustering is the dominant factor of the relaxation in region II, the relaxation time τ_{II} must be of the same order with the lifetime of such clusters.

To confirm the prediction above, we calculate the lifetime of the clusters of the A particles trapped in the cage. In order to define clusters without ambiguity, we use the Voronoi polygon.[58] A Voronoi polygon is a region associated to each of the particle and is defined as a set of points whose nearest particle is the center particle of the Voronoi polygon. By this definition, the system is spatially divided into Voronoi polygons uniquely. In what follows, a set of Voronoi polygons is called a domain if the set consists of Voronoi polygons of the same species and any of the polygons in this set has at least one contiguous polygon which belongs to the set. If the domain is enclosed by domains of the different species, the domain is called a cluster. The size of the cluster is given by the number of particles in the cluster.

In Fig. 5.10 we show examples of the domain structure around a specified A particle, which is indicated by a large solid circle at the center of each figures, at four different times $t = -1.0$, 0.0, 1.0 and 2.0 for the case $n\sigma^2 = 0.770$ and $c_R = 0.75$. Here the time t is set equal to zero at the time when the compression wave front passes over the specified particle. In the figures the open Voronoi polygons, the shaded polygons and the dark polygons show those which correspond to S, A and B

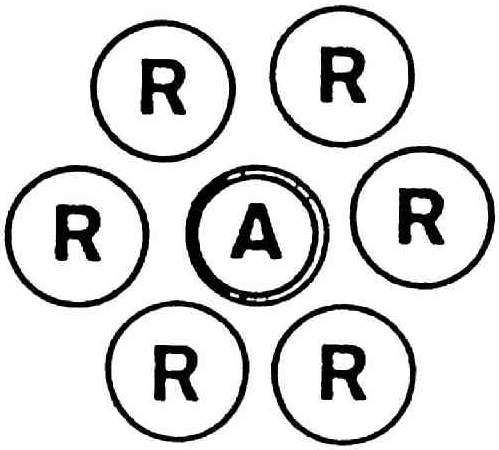

Fig. 5.9

A cage which is composed of only reactive species (A and B) and no catalyst (S) is shown. In this figure, particles marked as "R" represent particles of species A or B. The center A particle has less opportunity to experience reactive type collision (A + S type collision) than the average.

particles, respectively. At t = -1.0 small or one-particle S-clusters are embedded in a large domain of A particles. At t = 0.0 as a result of reactions between A and S particles, B-clusters are created in the left-half of the A-domain as shown in Fig. 5.10(b). As time goes further, the reactions proceed and resultant B particles make small B-clusters form a large B-domain. The domain structure at t = 2.0 shows the pattern after all reactive collisions ceased (Fig. 5.10(d)). There are several A particles which are enclosed by B particles and hence have no opportunities to make reactive collisions with S particles. As a result these A particles survive for a considerably long period. In this way for the case c_R = 0.75 the relaxation processes after the passage of the wave front may be sketched as destruction and shrinkage of the A-domain and the diffusion of S particles into A and B-clusters.

On the other hand, in case of c_R = 0.9, the situation becomes rather different. In Fig. 5.11, similar snapshot pictures of the Voronoi polygons to those in Fig. 5.10 are shown for the case $n\sigma^2$ = 0.770 and c_R = 0.9. In Fig. 5.11(c) it is shown that there remains considerably large clusters of A particles compared to the case c_R = 0.75 (Fig. 5.10(c)). In this case we consider the relaxation process as the nucleation and growth process of created B particles from the dispersed center of S particles rather than as the shrinkage process of the A-clusters.

To see whether the process of the shrinkage of the A-clusters is the dominant factor of region II or not, we

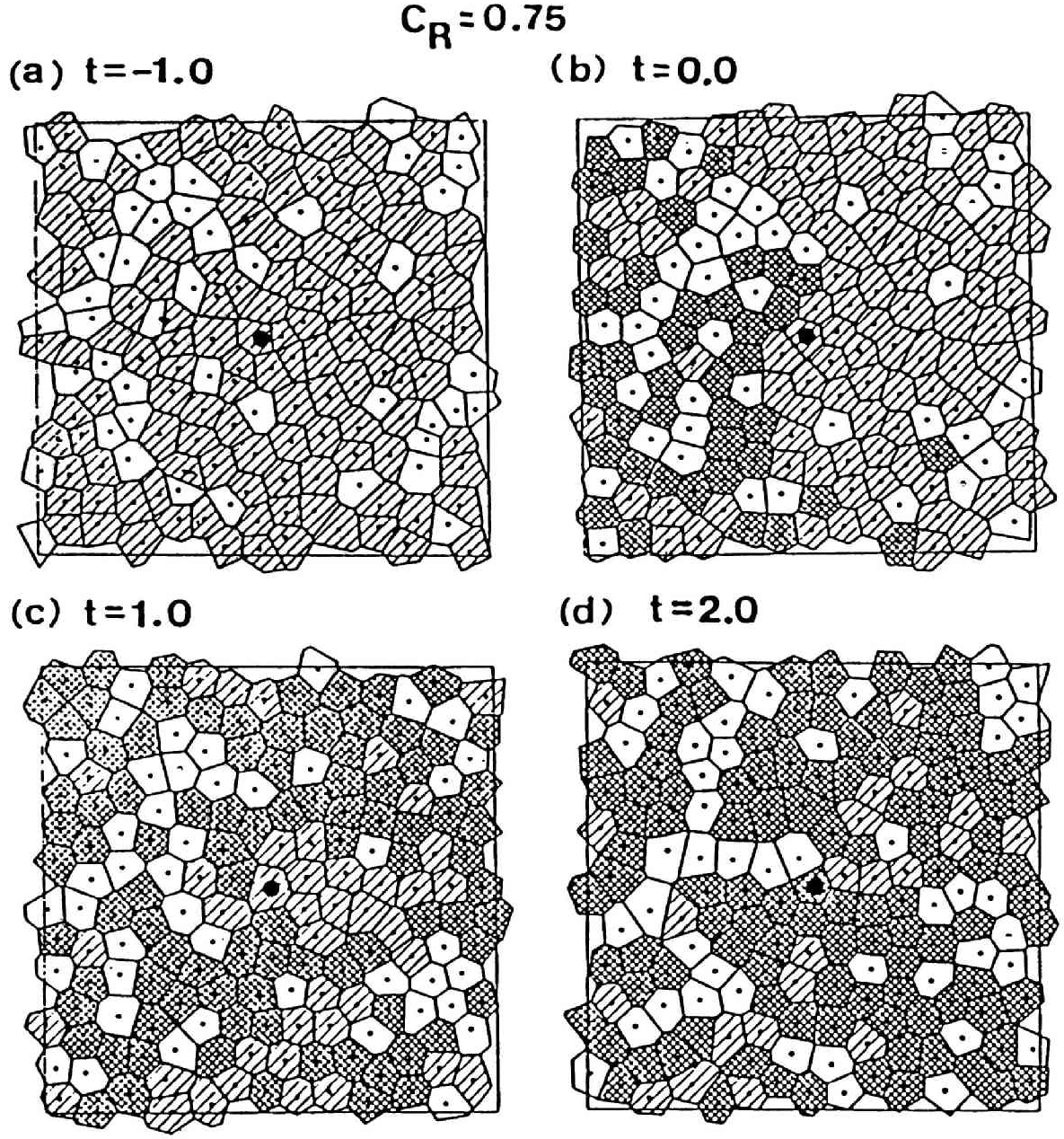

Fig. 5.10

Time evolution of the clusters of surviving A particles are shown for the case $n\sigma^2 = 0.770$ and $c_R = 0.75$ using the Voronoi polygons. The open Voronoi polygons, the shaded polygons and the dark polygons show those of the S, A and B particles, respectively.

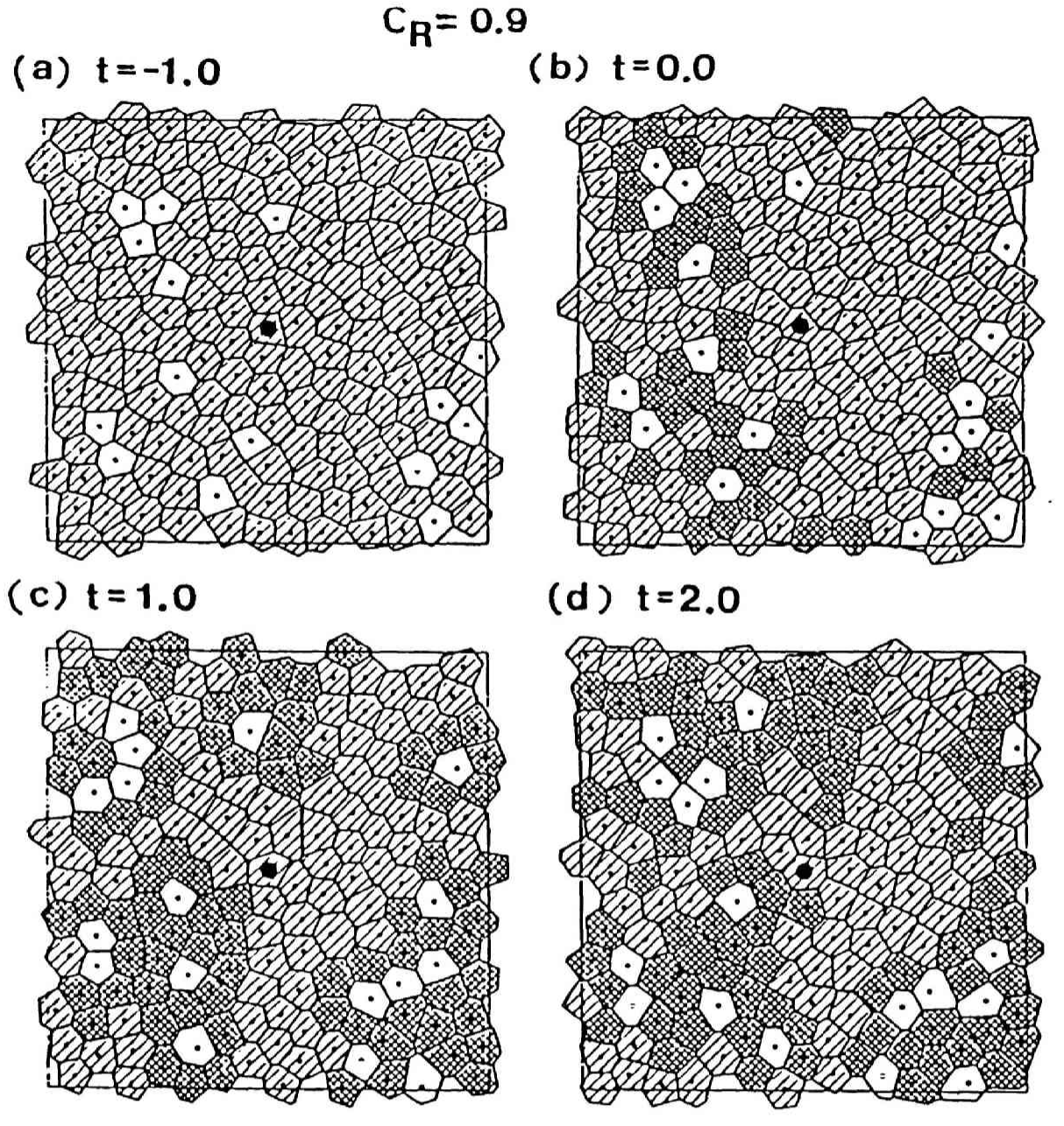

Fig. 5.11

Similar snapshot pictures of the Voronoi polygons to those in Fig. 5.10 are shown for the case $n\sigma^2 = 0.770$ and $c_R = 0.9$.

calculate the time evolution of the average cluster size of the surviving A particles $\bar{n}(t)$, and the results are shown in Fig. 5.12 using semi-log plot for the case (a) $n\sigma^2 = 0.770$ and $c_R = 0.75$ and (b) $n\sigma^2 = 0.770$ and $c_R = 0.9$, respectively. Here in the definition of the A-cluster, the A particles which have contiguous S particles are not included in the member of the cluster because we are interested in the clusters of A particles which are trapped in a cage and have no opportunity to experience reactive type collisions.

In Fig. 5.12, ensemble average was taken over all the clusters observed in the system at various time, and the time in the figure is measured from the time when the wave front passes over the center particle in the cluster, which is defined as the nearest particle to the center of mass of the cluster. After the wave front passes through the cluster, the mean cluster size begins to decrease exponentially. The relaxation times calculated from these data are shown in Fig. 5.5(b) with crosses. For $c_R = 0.75$, relaxation time of the mean cluster size agrees with that of the chemical energy relaxation in the region II. This means that the process of cluster shrinkage well describes the slow relaxation in the region II. On the other hand, for $c_R = 0.9$, the relaxation time of the mean cluster size does not agree with τ_{II}. As was shown in Fig. 5.11, the picture of cluster shrinkage is not appropriate in this very large c_R region.

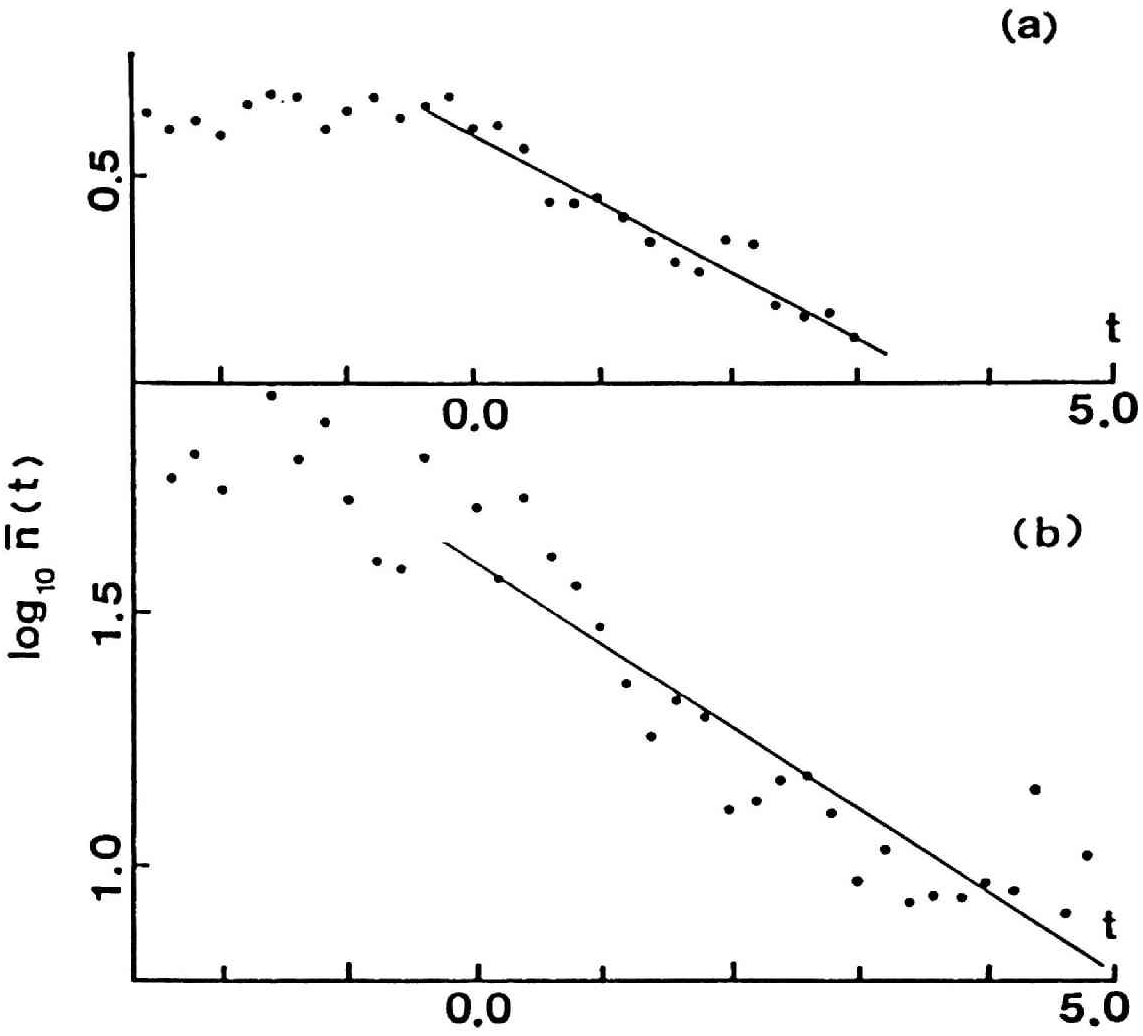

Fig. 5.12

Decay processes of the averaged cluster size of A particles are shown in semi-log plot for the case (a) $c_R = 0.75$ and (b) $c_R = 0.9$, both for $n\sigma^2 = 0.770$. Relaxation times of the region $t \geq 0$ are shown in Fig. 5.5(b) with crosses.

§ 5.5 Concluding Remarks

We found that the energy relaxation processes at the detonation wave front are composed of two different time regions. In the first region, progress of the reaction process is mainly determined by the rapid and non-correlated reactive collisions. In the late stage, two mechanisms compete. One is the relaxation of the temperature, and the other is the cage effect. In the latter case, the lifetime of the clusters due to diffusion process is much longer than the time scale of the element process of the reaction. Then the reaction process is regarded as a diffusion controlled reaction and the correlation between the collisions comes to be dominant in the time evolution of the whole system. This problem will be further investigated in the next chapter.

CHAPTER VI

FLUCTUATION DOMINATED KINETICS IN THE NON-EXOTHERMIC AND THE EXOTHERMIC REACTION SYSTEMS

§ 6.1 Introduction

When the time scale of the elementary process of the reaction is negligibly small compared to that of the diffusive motion of the reactive particles until they contact, the dynamical processes of this system are limited by the diffusion process and, therefore, this type of reaction is called the diffusion controlled reaction. In such system, the spatial fluctuations in the initial density distribution of the particles decay very slowly and survive even in the late stage of the reaction process. Therefore such fluctuations dominate the late stage dynamics and the behavior of the system does not obey the so-called rate equation, which assumes the system to be spatially homogeneous throughout the reaction process. The fluctuation dominated kinetics in the diffusion controlled reaction systems has recently been extensively investigated.[5,42-49] As the model reaction, 1) the radical recombination reaction $A + A \rightarrow 0$, 2) the particle-antiparticle recombination reaction $A + B \rightarrow 0$ and 3) the unimolecular trapping reaction $A + S \rightarrow S$ have been often employed

and the long time behavior of these systems has been studied. On each of these examples, anomalous long time tail of the decay process of the total number density of the species A has been theoretically predicted and confirmed by the Monte Carlo simulations.

As an example we mention the unimolecular trapping reaction. The unimolecular trapping reaction is expressed as

$$A + S \rightarrow S. \tag{6.1.1}$$

In the reaction (6.1.1), the A particles can be regarded as being trapped by the perfect sink S, which is left unchanged after trapping an A particle. A lot of investigations on the fluctuation dominated kinetics of reaction (6.1.1) have been performed with the assumption that the sink S is static and uniformly distributed.[47-49] If we assume that each of the species A and S distributes homogeneously at any time, then the total number density of the A particles at time t, denoted as $\rho_A(t)$, obeys the rate equation

$$\frac{\partial \rho_A(t)}{\partial t} = - k \rho_A(t) \rho_S, \tag{6.1.2}$$

where k is a reaction rate constant and ρ_S denotes the total number density of the S particles which is invariant through the reaction process. The rate equation (6.1.2) gives the decay law of $\rho_A(t)$ as

$$\rho_A(t) \sim \exp(-kt). \tag{6.1.3}$$

On the other hand, if we take into account the spatial inhomogeneity it is demonstrated that the long time behavior of $\rho_A(t)$ decays as

$$\rho_A(t) \sim \exp(-\kappa t^{d/(d+2)}), \tag{6.1.4}$$

where κ is a constant which depends on the initial number density of species A and d is the spatial dimension.[47-49] The anomalous decay law (6.1.4) originates from the fact that there exists an arbitrary large trap free region in which no trap S exists and the A particles can continue the random walks without being trapped for a long period.

As was seen in the preceding chapter the microscopic fluctuations in the particle distribution play an essential role in the late stage dynamics of our reacting system, when the system enters into the diffusion controlled regime. In this chapter we focus our attention to the fluctuation effects on the late stage dynamics and perform a series of MD runs to investigate such effects separately.

§ 6.2 Rate Equation Analysis for Our Model

As was discussed in chapter V, the slow relaxation of the energy after the detonation wave front passes is composed of two

factors, one is the temperature relaxation and the other is the spatial inhomogeneity. The former factor originates from the increase of the reverse reactions near the equilibrium and we are not interested in this factor at present. In order to concentrate on the latter factor, we suppress the reverse reaction in our model reaction and consider an irreversible reaction expressed as

$$A + S \rightarrow B + S + \Delta Q. \qquad (6.2.1)$$

In this reaction, the created B particles do not affect the reaction dynamics and can be identified with the inert species. Therefore the reaction (6.2.1) is reduced to the unimolecular trapping reaction (6.1.1). The differences between our model reaction and that used in the above investigations[47-49] are that the trap S is mobile in our model and our reaction is accompanied by the release of the reaction heat ΔQ. Therefore, on analyzing the behavior of the particle number in our system, we must consider the temperature change simultaneously.

Before performing the MD experiments, we present the results of analysis using the rate equation for the reaction (6.2.1). The rate equation for the reaction (6.2.1) is

$$\frac{\partial \rho_A(t)}{\partial t} = - k(T)\ \rho_A(t)\ \rho_S, \qquad (6.2.2)$$

which is the same as eq. (6.1.2). But in this case, as the reaction (6.2.1) is exothermic reaction, the temperature changes as the reaction process proceeds. Therefore the reaction rate constant k depends on the temperature T as

$$k(T) = k_0 \; T^{1/2} \exp\left(- \frac{\varepsilon}{k_B T} \right) , \qquad (6.2.3)$$

where k_0 is a constant which depends on the total number density of the particles. The factor $\exp\left(- \frac{\varepsilon}{k_B T} \right)$ is the usual Boltzmann's factor and the factor $T^{1/2}$ originates from the fact that the collision frequency is proportional to the mean velocity of the particles and therefore proportional to $T^{1/2}$. We can determine the temperature at time t, denoted as T(t), as a function of $\rho_A(t)$. The conservation relation of the total energy is expressed as

$$n k_B T_0 + \Delta Q \; \rho_A(0) = n k_B \; T(t) + \Delta Q \; \rho_A(t), \qquad (6.2.4)$$

where $\rho_A(0)$ is the number density of the A particles at the initial time and n is the total number density. Substituting eqs. (6.2.3) and (6.2.4) into the rate equation, eq (6.2.2), leads to the closed equation for $\rho_A(t)$ as

$$\frac{d\rho_A(t)}{dt} = - k_0 \rho_S \rho_A(t) \{ T_0 + (\rho_A(0) - \rho_A(t)) \frac{\Delta Q}{nk_B} \}^{1/2}$$

$$\times \exp(- \frac{\varepsilon}{k_B T_0 + (\rho_A(0) - \rho_A(t)) \Delta Q/n}). \quad (6.2.5)$$

By solving eq. (6.2.5), we can predict the time evolution of $\rho_A(t)$ under the assumption that the system is always homogeneous.

As we are now interested in the long time behavior of the system, the asymptotic form of the solution of the eq. (6.2.5) will be important. As $\rho_A(t)$ decays monotonically to zero, we can assume that $\rho_A(t) << 1$ when $t \to \infty$. Therefore, expanding eq. (6.2.5) in powers of $\rho_A(t)$ and retaining the leading term we have

$$\frac{d\rho_A(t)}{dt} = -k_0\rho_S(T_0 + \rho_A(0)\frac{\Delta Q}{nk_B})^{1/2}\exp(- \frac{\varepsilon}{k_B T_0 + \rho_A(0)\Delta Q/n}) \rho_A(t), \quad (6.2.6)$$

which leads to the exponential decay law of $\rho_A(t)$ irrespective of the values of each of the parameters.

§ 6.3 MD Experiments and Simple Theoretical Interpretations

We performed the MD experiments on the fluctuation effects on the late stage dynamics as follows: The system is a square box and the periodic boundary condition is imposed on each of the sides. The initial state is a mixture of the A and the S particles uniformly distributed in the box. The particle numbers of the species A and S in the initial state, N_A and N_S, is in the ratio $N_A : N_S = c_R : 1 - c_R$, and, therefore, $\rho_A(0) = c_R$. From this initial state, we calculate the time evolution of the system following the reaction (6.2.1) and the decay process of $\rho_A(t)$ is observed for the parameters listed in Table 6-I. The density of the system is taken to be high density ($n\sigma^2 = 0.770$) in which the fluctuation effects is expected to be important.

In Fig. 6.1 we present the MD results of the decay process of $\rho_A(t)$ in the normal plot and the semi-log plot along with the results of the rate equation (6.2.5) for the case a) $\varepsilon = 0.0$, $\Delta Q = 0.0$ and $c_R = 0.5$ and b) $\varepsilon = 3.0$, $\Delta Q = 3.0$ and $c_R = 0.5$, respectively. We find that the rate equation well describes the early stage behavior of $\rho_A(t)$. In the late stage, on the other hand, the decay rate of the system becomes slower than that predicted by the rate equation, which is suggestive of the effects of the spatial inhomogeneity. Such discrepancy between the results of the MD and the rate equation was also obtained for the other sets of parameters listed in Table. 6-I.

We can give an intuitive explanation to this slow decay process following Balagurov and Vaks.[47] If the molar fraction

Table 6-I The parameters used for the MD runs to study the fluctuation effects in the irreversible reaction A + S → B + S + ΔQ. MD runs were done on the N = 9752 system.

$n\sigma^2$	ε	ΔQ	c_R
0.770	0.0	0.0	0.25[a)]
			0.50[a)]
			0.75
			0.90
	3.0	3.0	0.25
			0.50
			0.75
			0.90

a) In these cases, the MD runs were done on the N=28080 system.

a)

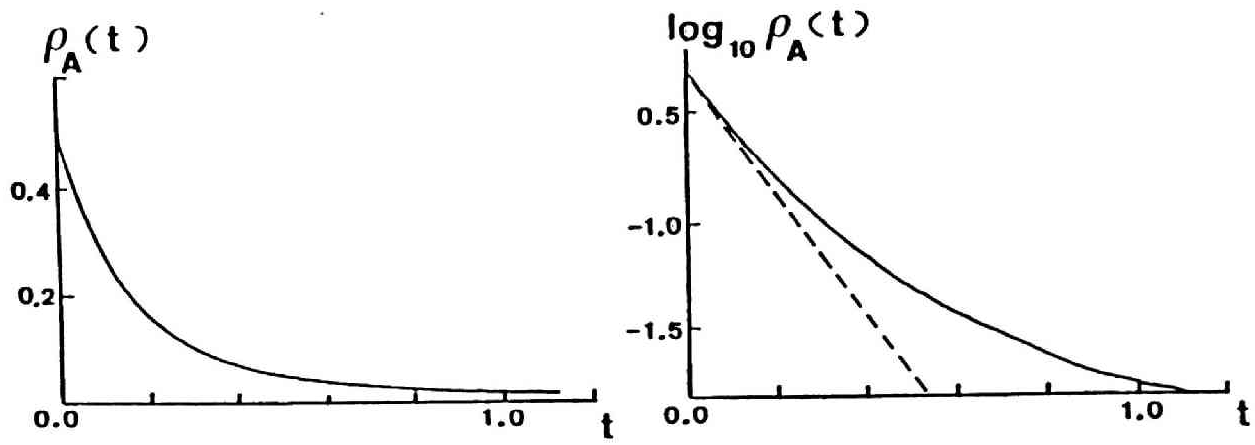

b)

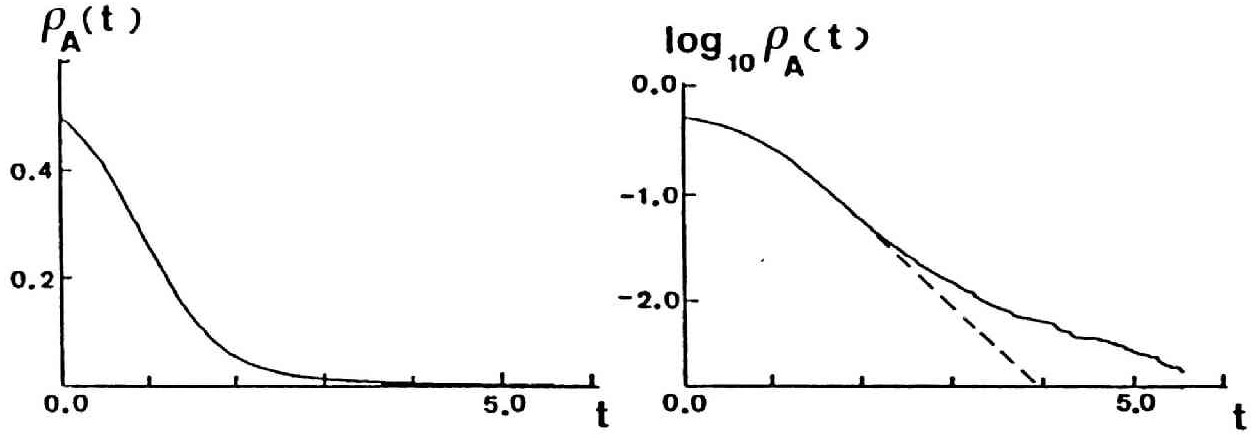

Fig. 6.1

The MD result (solid lines) and the prediction of the rate equation (6.2.5) (broken lines) of the decay processes of $\rho_A(t)$, the total number density of the species A, are presented for the case a) $\varepsilon = 0.0$ and $\Delta Q = 0.0$ and b) $\varepsilon = 3.0$ and $\Delta Q = 3.0$. The density is $n\sigma^2 = 0.770$ and the initial molar fraction of the species A is $c_R = 0.5$. It can be found that the rate equation does not give the correct behavior in the late stage.

of the species A is not so large, the system can be regarded to be composed of many clusters of A particles (hereafter we call such clusters as the A-clusters). As we assign species to each particle randomly in the initial state, the probability that we find a region of area ℓ^2 in which all of the particles are A's obeys the Poisson distribution. Therefore, the probability of finding an A-cluster of linear dimension ℓ, say $f(\ell)$, obeys the Gaussian distribution:

$$f(\ell) = 2 \left(\frac{C}{\pi}\right)^{1/2} \exp(- C\ell^2), \tag{6.3.1}$$

where C is a function of the mean separation distance λ between the particles

$$C = - \frac{1}{\lambda^2} \ln c_R \qquad (> 0) . \tag{6.3.2}$$

As the reaction process proceeds, each of the A-clusters shrinks and the number of the A particles contained in a cluster decreases monotonically. Now we define $\Phi_\ell(t)$ as the number of the A particles per cluster at time t averaged over the A-clusters whose initial linear dimensions are ℓ. If we assume that the decay of the A-clusters, which existed in the initial state, dominates the density variation $\rho_A(t)$ in the late stage, $\rho_A(t)$ can be given by averaging over all the A-clusters which initially existed as

$$\rho_A(t) \sim \int_0^\infty f(\ell)\ \Phi_\ell(t)\ d\ell\ . \qquad (6.3.3)$$

Here we neglected the constant factor because we are interested in the qualitative behavior of $\rho_A(t)$. We must determine the decaying law $\Phi_\ell(t)$. If the species S is static and distributes uniformly, it is known that $\Phi_\ell(t) \sim \exp(-Dk_0^2 t)$, where D is the diffusion constant of the particles and k_0 is the smallest possible wave number inside the cluster and is the order of $1/\ell$.[47] As the S particles are mobile in our case, the decay law of the clusters must be, at the slowest, exponential function of time. We performed a series of MD experiments on the decay process of the circular domain of A particles isolated in the sea of the S particles. A typical example is shown in Fig. 6.2. In this figure the spatial distribution of the A particles are shown. From the results of such MD runs, we confirmed that the circular domain decays exponentially in time. The relaxation time of the domain of size ℓ, denoted as τ_ℓ, can be estimated by the time during which the diffusion length becomes to be the size of the cluster:

$$(D\,\tau_\ell)^{1/2} \sim \ell\ . \qquad (6.3.4)$$

Therefore we obtain the decay law of the cluster as

$$\Phi_\ell(t) \sim \exp(-Dt/\ell^2)\ . \qquad (6.3.5)$$

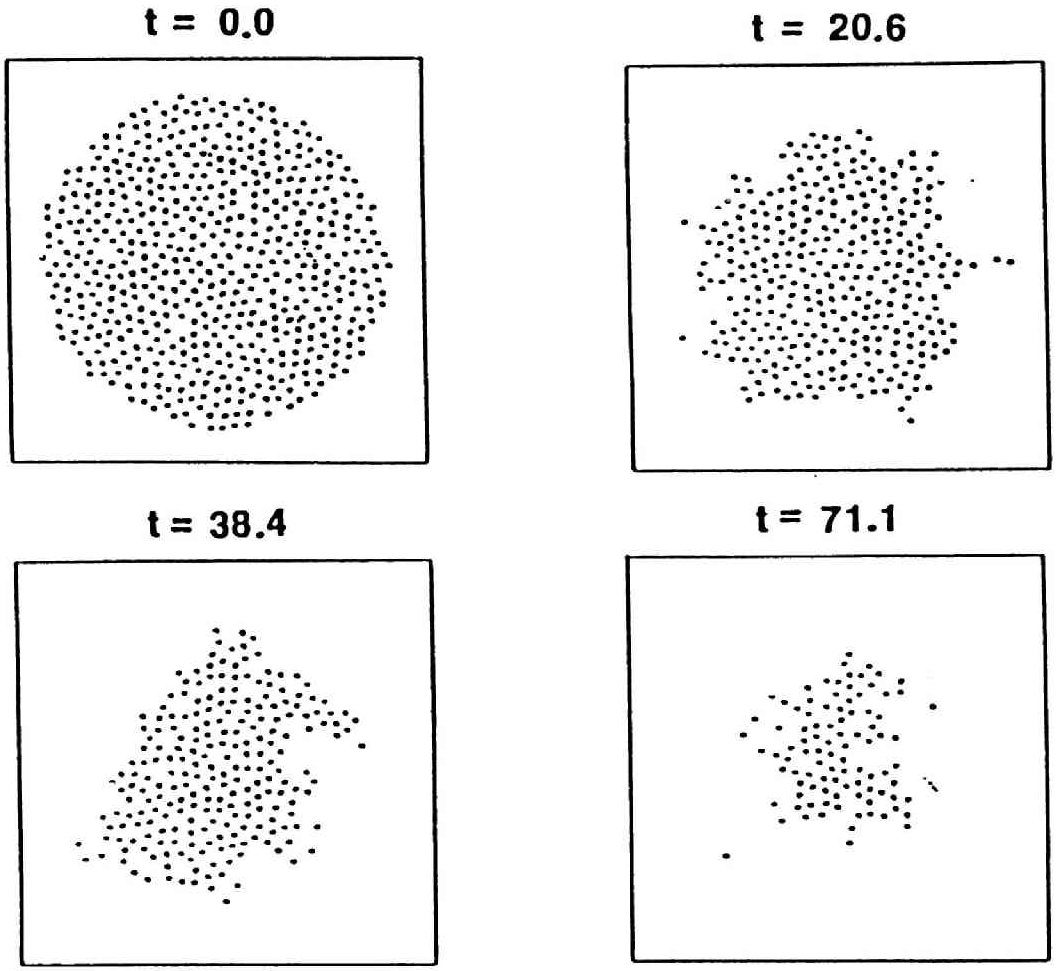

Fig. 6.2

A typical example of the decal process of a circular domain of the A particles located in a sea of the S particles is presented. Here, the spatial distribution of the A particles is presented and the parameters are chosen as $n\sigma^2 = 0.770$ and $\varepsilon = 0.0$ and $\Delta Q = 0.0$.

Substituting eq. (6.3.5) into the eq. (6.3.3), we obtain the long time behavior of $\rho_A(t)$ as

$$\rho_A(t) \sim \exp(- 2 \sqrt{CDt}) \ , \qquad (6.3.6)$$

which is slower than exponential. In Fig. 6.3 we plot log $\rho_A(t)$ versus $\sqrt{t}$ in order to check the prediction (6.3.6). The linearity of the curve is made better than that of Fig. 6.1, which suggests the cluster picture mentioned above.

If the system size is finite as the system used in the MD experiments, there is an upper cut-off of the distribution of the cluster size, say ℓ_c. Then, the upper limit of the integral in eq. (6.3.3) must be replaced by ℓ_c and the resulting decay law is as follows:

$$\rho_A(t) \sim \begin{cases} \exp (- 2 \sqrt{CDt}) & (t < t_c) \\ A\ell_c \dfrac{C^{1/2} \ell_c^{\,2}}{2(Dt)^{3/2}} \exp(- \dfrac{1}{C^{1/2} \ell_c^{\,2}} (Dt)^{3/2}) & (t > t_c), \end{cases} \qquad (6.3.7)$$

where $t_c \simeq C\ell_c^{\,2}/D$ and A is the normalization constant defined as

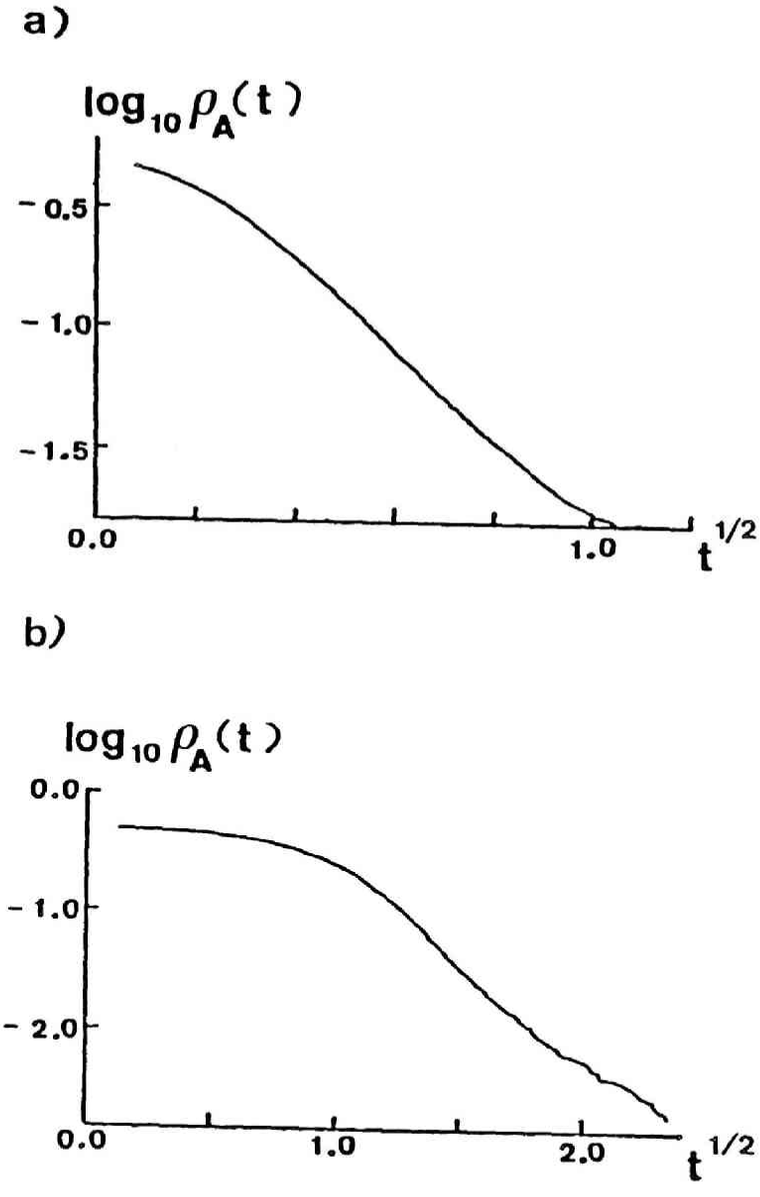

Fig. 6.3

The MD results of the decay processes of $\rho_A(t)$, that were presented in Fig. 6.1, are shown in the $\log_{10} \rho_A(t)$ versus $\sqrt{t}$ plot in order to test the decay law $\rho_A(t) \sim \exp (- \kappa t^{1/2})$, where κ is a constant.

$$A = \int_0^{\Omega_c} \exp(- C\Omega^2) \, d\Omega \, . \qquad (6.3.8)$$

As the exponential decay predicted by the rate equation (6.2.6) is slower than the long time tail of eq. (6.3.7), the system regains the exponential decay in the time region $t > t_c$. This behavior is also confirmed by the MD calculations (see Fig. 6.4).

§ 6.4 Concluding Remarks

The fluctuation in the particle number density was found to dominate the late stage of the decay process of $\rho_A(t)$ in a manner that the above naive theory predicts in both the non-exothermic and the exothermic reaction systems. We could not detect the characteristics of the exothermic reaction in this problem. This originates from the fact that in the late stage the effects of the reaction heat are negligible because the reaction events scarcely take place and therefore the system can be regarded as the non-exothermic reaction system.

Further investigations on the dynamical aspects of the fluctuation effects on the other type of reaction systems, such as the particle-antiparticle annihilation reaction $A + B \rightarrow 0$, in which the segregation of the species A and B emerges in the late stage,[5] and the radical recombination reaction $A + A \rightarrow 0$ are left to be done in future.

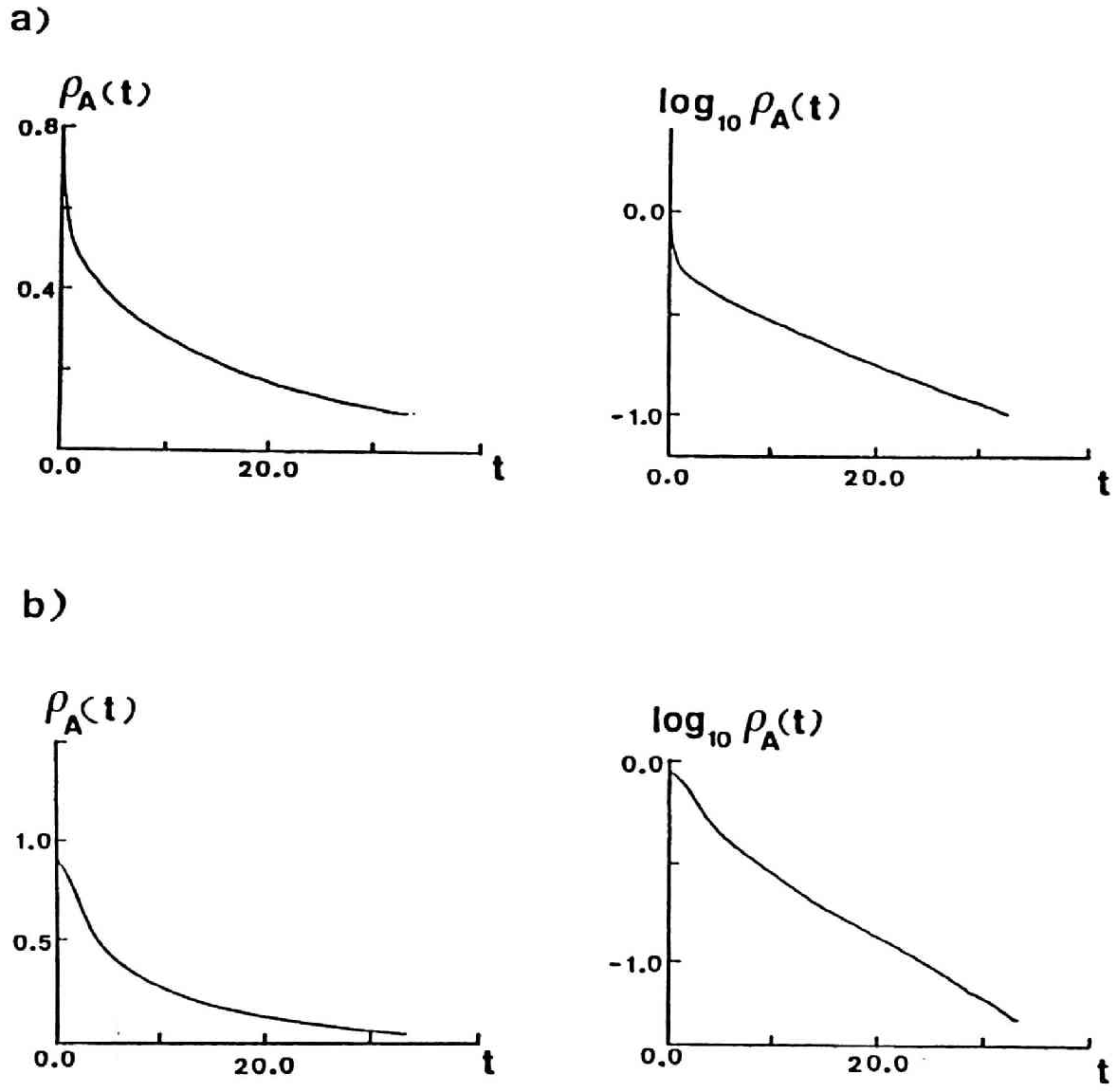

Fig. 6.4

The MD results of the decay processes of $\rho_A(t)$ are shown for the case a) $\varepsilon = 0.0$ and $\Delta Q = 0.0$ and b) $\varepsilon = 3.0$ and $\Delta Q = 3.0$. The density is $n\sigma^2 = 0.770$ and the initial molar fraction of the species A is $c_R = 0.9$. It can be found that the exponential decay law that is predicted by the rate equation is regained in the late stage.

CHAPTER VII

EFFECTS OF THE ACTIVATED COMPLEX WITH FINITE LIFETIME

§ 7.1 Introduction

In the previous chapters, we used a reactive hard disk system to model the exothermically reacting particles. Our main purpose is to understand how this simple model realizes the properties of the real reaction systems and what is the essential features of the reaction dynamics. For this purpose we adopted a model of an exothermic isomerization reaction

$$A + S \underset{\leftarrow}{\overset{\rightarrow}{}} B + S + \Delta Q \ , \qquad (7.1.1)$$

which occurs on the two body collisions between the reactive pair of the hard disks. Here the species A and B are isomers, S is the catalyst and ΔQ is the reaction heat of the forward reaction. We studied the detonation propagation phenomena using the model reaction (7.1.1) by MD method. It was shown that as long as the S particles are abundant in the system the detonation wave propagates stationarily with the velocity predicted from the hydrodynamic considerations and that the structure of the detonation in our MD experiments is similar to that of the real

detonation (chapters IV and V). The dynamical properties of the particles were also studied by calculating the energy relaxation processes at the detonation wave front (chapter V). By these works it was established that the simple reaction model, the hard disk system combined with the model reaction (7.1.1), can reproduce the main features of the detonation.

In this chapter we focus our attentions to the effects of the finite lifetime of the activated complex which is neglected in the model reaction (7.1.1). When the activated complex A^* is introduced in the model as

$$A \underset{\leftarrow}{\overset{\rightarrow}{}} A^* \underset{\leftarrow}{\overset{\rightarrow}{}} B + \Delta Q, \qquad (7.1.2)$$

the structure of the wave front and the energy relaxation processes are expected to be different from those of model (7.1.1) and to have more realistic features.

We summarize the model of the MD experiment in the next section and the results and the discussions are presented in § 7.3. In the final section § 7.4 we conclude this chapter.

§ 7.2 Summary of the Model

In order to introduce the activated complex A^* into our reactive hard disk model, we regard that the reaction (7.1.2) is composed of following set of reactions;

$$A + S \rightarrow A^* + S \qquad (7.2.1)$$

$$B + S \rightarrow A^* + S \qquad (7.2.2)$$

$$A^* + X \rightarrow A + X$$
$$\rightarrow B + X, \qquad (7.2.3)$$

where X denotes A, B or S species. We assume that the A^* is created by a collision between A and S or B and S and has the excess internal energy compared with either A or B (reactions (7.2.1) and (7.2.2)). The activated complex A^* thus created turns to the stable (or metastable) B or A species by releasing the excess energy through collisions with another particle (reaction (7.2.3)). By these assumptions, the reactions (7.2.1) and (7.2.2) are endothermic and the reaction (7.2.3) is exothermic. In these schemes, we neglect the possibility of the occurrence of the reactive collisions between two A^* particles such as $A^* + A^* \rightarrow B + A^*$. We neglect such process so as not to introduce any nonlinearity (nonlinear terms in the reaction rate equations) into the reactions (7.2.1)-(7.2.3), because we wish to construct a simple extension of the model reaction (7.1.1) keeping the linearity of the rate equation. As the A^* particles are short-lived in our model as will be shown below, $A^* + A^*$ type collisions are expected to be negligible and we can justify above assumption.

We present the schematic representations of the internal energy levels of the species A, B and A^* in Fig 7.1 for a) $A \underset{\leftarrow}{\rightarrow} B$

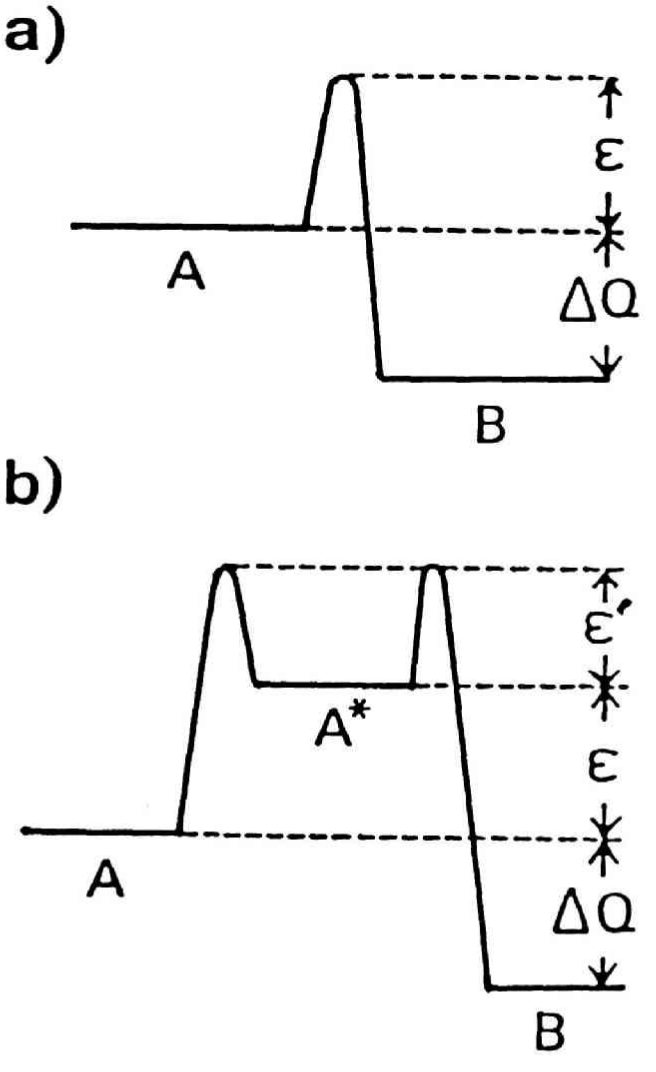

Fig 7.1 Schematic representations of the internal energy levels of each of the species are shown for a) A $\underset{\leftarrow}{\overset{\rightarrow}{}}$ B reaction (7.1.1) and b) A $\underset{\leftarrow}{\overset{\rightarrow}{}}$ A* $\underset{\leftarrow}{\overset{\rightarrow}{}}$ B reaction (7.2.1)-(7.2.3).

reaction (7.1.1) and b) $A \underset{\leftarrow}{\overset{\rightarrow}{}} A^* \underset{\leftarrow}{\overset{\rightarrow}{}} B$ reaction (7.2.1)-(7.2.3). If the reactive type pair collides and the head-on collision component of the relative kinetic energy exceeds the activation energy ($\varepsilon + \varepsilon'$ for (7.2.1), $\varepsilon + \Delta Q + \varepsilon'$ for (7.2.2) and ε' for (7.2.3)), the reaction takes place and the reaction heat ($-\varepsilon$ for (7.2.1), $-(\varepsilon + \Delta Q)$ for (7.2.2) and ε or $\varepsilon + \Delta Q$ for (7.2.3)) is released to the kinetic energy of the colliding two particles. Here we assume that each of the two open channels in reaction (7.2.3) is selected randomly with an equal possibility. In this model an activated complex A^* has a finite lifetime which is of the same order as the mean free time of the particles as long as the activation energy ε' for the reaction (7.2.3) is comparable to the mean kinetic energy per a particle.

The methods of the MD experiments used in this work are as follows. The system is an N hard disk system (N = 9000 or 28000) all with identical mass m and diameter σ contained in a rectangular box with sides L_x and L_y along which we take the x and y-coordinates. The ratio of the length of the side L_x to that of the side L_y is 20:1 for the case N = 9000 and 60:1 for the case N = 28000, respectively. The sides L_x's are assumed to be periodic boundaries and L_y's are to be elastic walls. First we prepare a thermal equilibrium state of the non-reactive hard disk system at temperature T_0 and with specified dimensionless particle number density $n\sigma^2$, where n is the particle number density, and we assign species A or S to each disk randomly with a uniform distribution so that the number of total A's and S's are in the ratio c_R:1-c_R. Then the velocities of all the

particles in the range $0 \leq x \leq \Upsilon L_x$ are multiplied by a factor 5.0 in order to initiate a detonation, where the value of Υ is 1/50.0 for N = 9000 case and 1/150.0 for N = 28000 case. The detonation wave thus initiated propagates along the x-direction and we calculate the detonation velocity and the energy relaxation processes at the detonation wave front from the MD data.

In the following all quantities are dimensionless with use of the units of length σ, mass m, time $(m\sigma^2/k_BT_0)^{1/2}$ and energy k_BT_0, where k_B is the Boltzmann's constant.

§ 7.3 The Results of the MD Experiments

As we are interested in the effects of activated complex A^* which has the finite lifetime, we performed a series of MD runs for the same parameters that were used for the previous $A \underset{\leftarrow}{\overset{\rightarrow}{}} B$ reaction in chapter V by changing ε', which determines the mean lifetime of A^*. The parameters used are listed in Tables 7-I and 7-II. In the MD runs listed in Table 7-I, we kept the parameters ε' to be 0.0. Therefore, an A^* turns to an A or a B at the first collision with another particle and the lifetime of A^* corresponds to the mean free time. In the runs in Table 7-II the lifetime of A^* increases as the values of ε' increase. Most of the computations are done for the N=9000 system except for a few cases in which we use N=28000 system to test the stability of the detonation for a long period.

Table 7-I The parameters used in the MD experiments and the MD results of the detonation velocity.

The parameters ε, ΔQ and ε' are 10.0, 40.0 and 0.0 respectively, and one computation run was performed for each set of parameters.

$n\sigma^2$	c_R	Detonation velocity (MD)
0.770	0.25	41.4
	0.50	53.0[a]
	0.75	55.8[a]
	0.90	49.8[a]
0.116	0.25	8.6[a]
	0.50	11.6[a]
	0.75	12.9[a]
	0.90	13.8[a]

a) For these cases the MD runs were done for both N=9000 and 28000 systems. The values of the MD detonation velocities presented in the table are determined using the N=28000 data.

Table 7-II The parameters used and the detonation velocities from a series of MD runs in which the lifetime of the activated complex A^* is changed.

In each case, the parameters ε, ΔQ, $n\sigma^2$ and c_R are 10.0, 40.0, 0.770 and 0.5 respectively, and one computation run was performed with N = 9000 system for each set of parameters.

$n\sigma^2$	ε'	Detonation velocity (MD)
0.770	0.0	53.0 a)
	10.0	50.5
	15.0	48.3 b)
	20.0	---- b)
0.116	0.0	11.6 a)
	10.0	10.8 b)
	15.0	---- b)
	20.0	---- b)

a) Results of N = 28000 system.

b) In each of these cases, the detonation did not propagate stationary.

Despite the fact that the lifetime of the A^*'s is of the order of the mean free time, the detonation propagates considerable distance during the lifetime of the A^*. Therefore it is expected that the A^*'s have the detectable effects on the velocity and the structure of the detonation.

First we consider the detonation velocity. In our MD runs we found that, different from the previous $A \underset{\leftarrow}{\overset{\rightarrow}{}} B$ reaction case, the detonation velocity increases slightly for a short period after its initiation. This transient period originates from the fact that more excess enthalpy is needed to construct a stable detonation in the $A \underset{\leftarrow}{\overset{\rightarrow}{}} A^* \underset{\leftarrow}{\overset{\rightarrow}{}} B$ reaction than in the $A \underset{\leftarrow}{\overset{\rightarrow}{}} B$ reaction because of the existence of the energetic A^*'s at and behind the wave front. After such transient period we can observe that the detonation propagate stationarily. We determined the detonation velocities from the MD data in the stationary region of the propagation and the results are also listed in Tables 7-I and 7-II. In Fig 7.2 we show, for the cases a) $n\sigma^2 = 0.770$ (high density fluid phase) and b) $n\sigma^2 = 0.116$ (low density fluid phase) both with $\varepsilon' = 0.0$, the comparison between the MD detonation velocities and the theoretical ones, for which we employed hydrodynamics as in chapter V. From Fig 7.2 the overall behavior is quite similar to that of the $A \underset{\leftarrow}{\overset{\rightarrow}{}} B$ reaction. We find the disagreement between the MD and the theoretical velocities in the high density and large c_R region, which originates from the cage effect mentioned in chapter V. Moreover, from the MD results of the detonation velocity in Table 7-II, it is seen that the detonation velocity is rather insensitive to the change in the

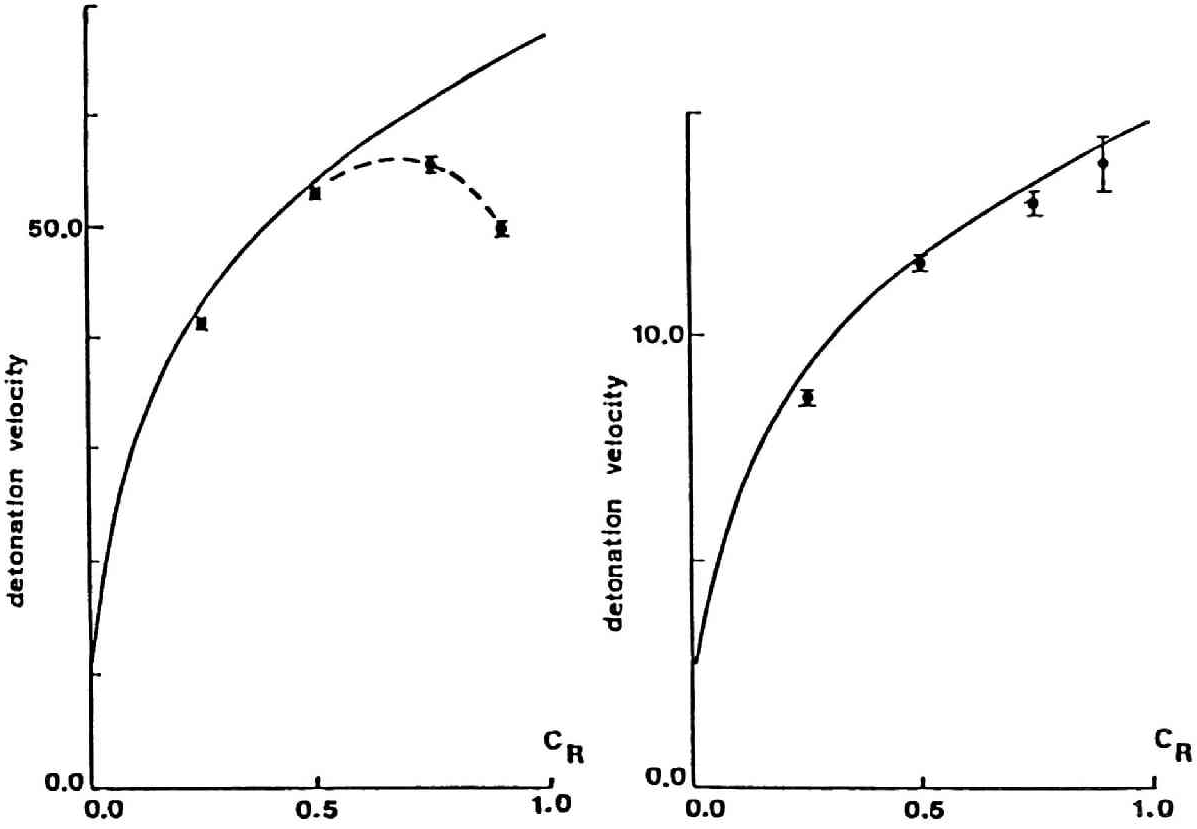

Fig 7.2 The detonation velocities obtained by the MD experiments (solid circles) and by the hydrodynamic theory (solid line) on the reaction $A \underset{\leftarrow}{\overset{\rightarrow}{}} A^* \underset{\leftarrow}{\overset{\rightarrow}{}} B$ are shown for a) $n\sigma^2 = 0.770$ and b) $n\sigma^2 = 0.116$. Here, c_R is the molar fraction of A particles at the initial state.

lifetime of A^* (the change of ε') and the detonation velocity decreases slightly as the lifetime of A^* increases (ε' increases). From these results we can conclude that the finite lifetime of A^* has an unimportant effect on the detonation velocity. It only determines the critical lifetime of A^* above which the detonation can no longer propagate stationarily.

Next we turn to the wave front structure. Now our attention is being paid mainly to the fact that the wave front structure of the detonation in the previous $A \underset{\leftarrow}{\overset{\rightarrow}{}} B$ reaction system deviates from that of the real detonation (chapter IV). The real detonation wave consists of two parts, one is the compression zone and the other is the reaction zone. The compression zone corresponds to the induction period in which the excess energy of the translational motion of the molecule activated by the passage of the shock wave front is transferred to the internal vibrational motion of the molecule which finally causes the exothermic reaction. After this induction period the actual isomerization reaction begins to proceed and this region is called as the reaction zone. Our previous MD experiment on the detonation in the $A \underset{\leftarrow}{\overset{\rightarrow}{}} B$ reaction system did not reproduce the compression zone and we considered that this character originates from the lack of the internal degrees of freedom in our hard disk reaction system $A \underset{\leftarrow}{\overset{\rightarrow}{}} B$ (chapter IV). In the $A \underset{\leftarrow}{\overset{\rightarrow}{}} A^* \underset{\leftarrow}{\overset{\rightarrow}{}} B$ reaction system, on the other hand, we expect that the activated complex A^* gives rise to the relaxation time for the energy transfer from the translational motion to the internal vibrational motion and

that this reaction system including A^* reproduces the wave front structure correctly.

In order to investigate this problem on the wave front structure we calculated the energy relaxation processes of the A particles at the detonation wave front, following the methods of calculation presented in chapter V. Now we define a quantity $\langle E(t) \rangle$ as an average total energy per particle at time t, where the time t is measured from the time when the wave front passes over the particle. Here the total energy $\langle E(t) \rangle$ is the sum of the chemical energy (potential energy) per particle $\langle E_p(t) \rangle$ and the kinetic energy per particle $\langle E_K(t) \rangle$. In Fig.7.3 we show how the $\langle E(t) \rangle$ changes during the passage of the wave front for the case $n\sigma^2 = 0.770$ and $c_R = 0.5$. Figure 7.3a) is for the $A \underset{\leftarrow}{\overset{\rightarrow}{}} B$ reaction with $\varepsilon = 10.0$ and $\Delta Q = 40.0$ and Figs 7.3b)-d) are for the $A \underset{\leftarrow}{\overset{\rightarrow}{}} A^* \underset{\leftarrow}{\overset{\rightarrow}{}} B$ reaction with $\varepsilon = 10.0$ and $\Delta Q = 40.0$ and $\varepsilon' =$ b) 0.0, c) 10.0 and d) 15.0 respectively. In these figures the time t = 0 corresponds to the time when the wave front passes over the observer. The most significant difference between the reactions $A \underset{\leftarrow}{\overset{\rightarrow}{}} B$ and $A \underset{\leftarrow}{\overset{\rightarrow}{}} A^* \underset{\leftarrow}{\overset{\rightarrow}{}} B$ is whether the total energy $\langle E(t) \rangle$ increases at the wave front (t=0.0) or not. As the $\langle E(t) \rangle$ is the sum of the $\langle E_p(t) \rangle$ and the $\langle E_K(t) \rangle$, we can analyze the above-mentioned behavior by decomposing the $\langle E(t) \rangle$ into these two components. In Fig 7.4 we present an example of the decomposition of the $\langle E(t) \rangle$ as shown in Fig 7.3b). As is seen from this figure the chemical energy per an initial A particle decays monotonically, which indicates the progress of the exothermic isomerization reaction $A \rightarrow B$. Therefore we can regard that the beginning of the

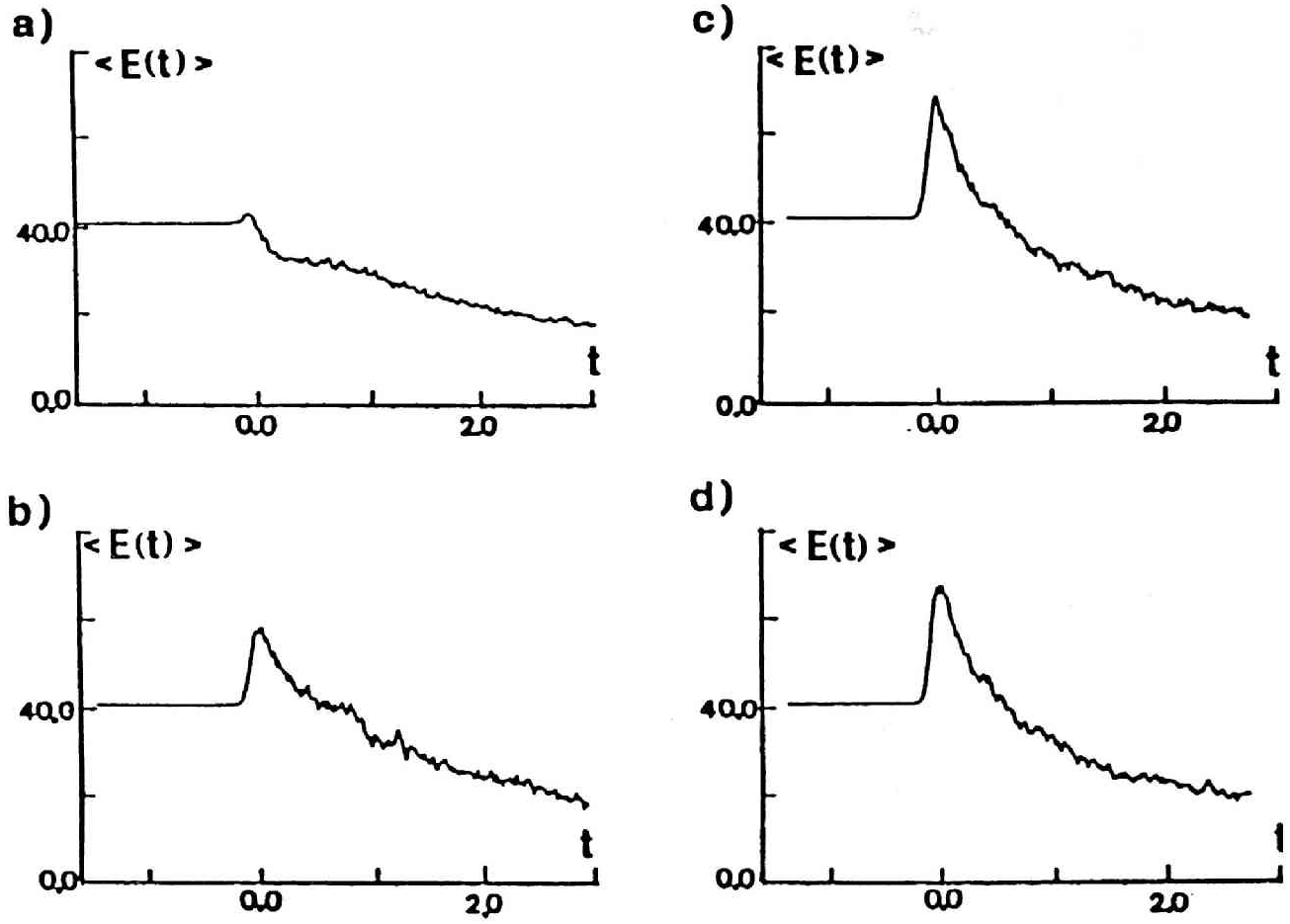

Fig 7.3 The time evolution of the total energy per particle, $\langle E(t) \rangle$ is shown for a) $A \underset{\leftarrow}{\overset{\rightarrow}{}} B$ reaction and b)-d) $A \underset{\leftarrow}{\overset{\rightarrow}{}} A^* \underset{\leftarrow}{\overset{\rightarrow}{}} B$ reaction. Here the parameters are chosen as $n\sigma^2 = 0.770$, $\varepsilon = 10.0$, $\Delta Q = 40.0$ and $c_R = 0.5$ for all cases and $\varepsilon' =$ b) 0.0, c) 10.0 and 15.0, respectively.

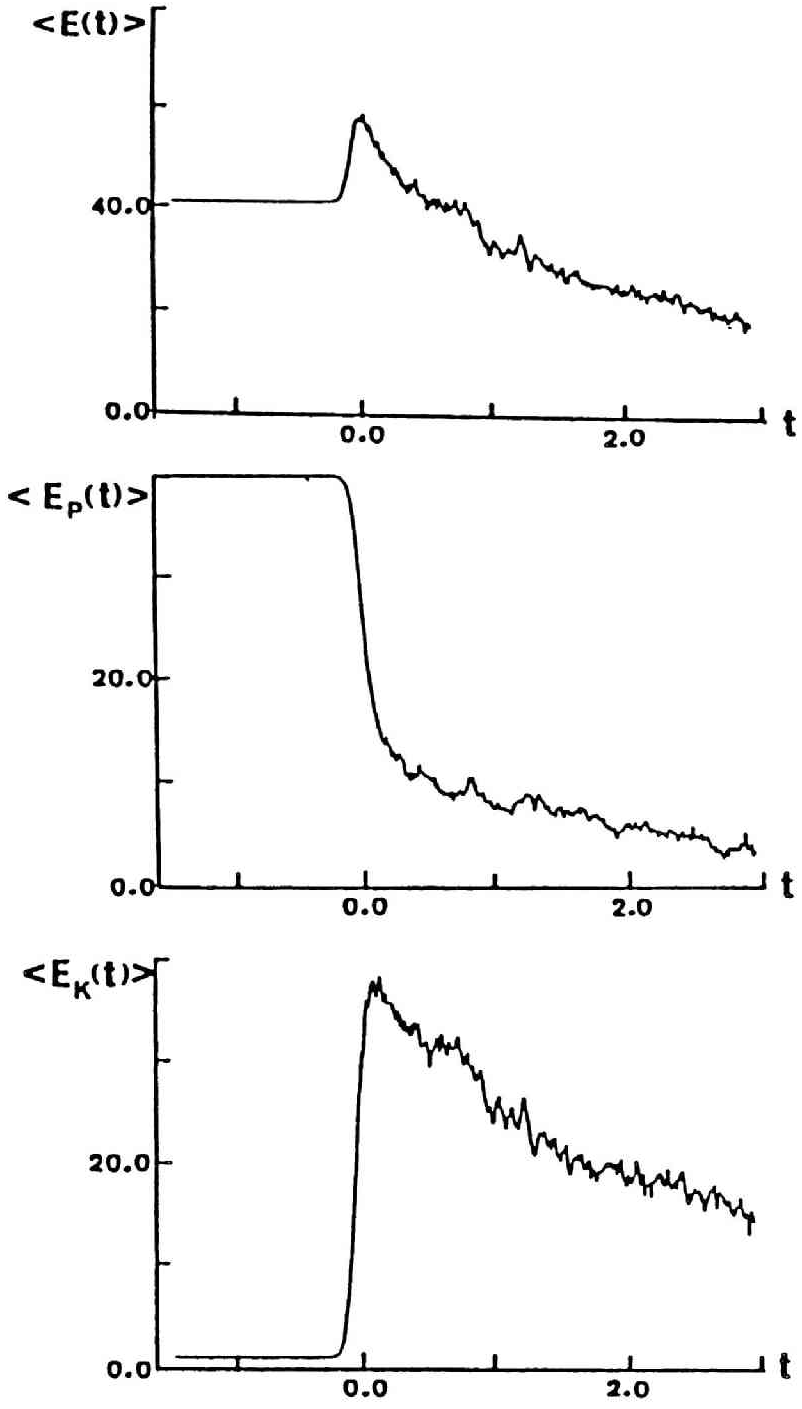

Fig 7.4 An example of the decomposition of the total energy $\langle E(t) \rangle$ into the chemical energy $\langle E_p(t) \rangle$ and kinetic energy $\langle E_k(t) \rangle$ is shown for the $\langle E(t) \rangle$ that is presented in Fig 7.3b).

decrease of $\langle E_p(t) \rangle$ corresponds to the passage of the reaction zone front. On the other hand, as the kinetic energy $\langle E_k(t) \rangle$ increases primarily by the shock compression, we can consider that the abrupt increase of the $\langle E_k(t) \rangle$ corresponds to the passage of the shock front. Combining these two effects it is understood that the increase of the $\langle E(t) \rangle$ means that the particle gains the excess energy from the shock compression of the detonation wave without losing its chemical energy by the reactive collisions and therefore the period in which the $\langle E(t) \rangle$ is increasing can be regarded as the compression zone. Returning to Fig. 7.3 we see that for the reaction $A \underset{\leftarrow}{\overset{\rightarrow}{}} B$ (Fig 7.3a) the $\langle E(t) \rangle$ decays almost monotonically. This means that for $A \underset{\leftarrow}{\overset{\rightarrow}{}} B$ reaction system there is no compression zone and the shock wave front coincides with the front of the reaction zone. For the reaction $A \underset{\leftarrow}{\overset{\rightarrow}{}} A^* \underset{\leftarrow}{\overset{\rightarrow}{}} B$ (Fig 7.3b-d), however, there exists a time interval in which the $\langle E(t) \rangle$ increases and this indicates the existence of the compression zone. The period of such time interval is about 0.3 (dimensionless time) and this corresponds to the width of the compression zone of about 15σ (because the detonation velocity is about 50). Therefore introducing A^* into the model makes the structure of the detonation more realistic.

§ 7.4 Concluding Remarks

As was seen in the preceding section, the existence of the activated complex A^* is not essential in the propagation

mechanism of the detonation. One of the effects of the A^* is the formation of the compression zone before the exothermic reactions begin. This point was the only difference between the real detonation and the MD detonation from the model (7.1.1) (chapter IV). Therefore we can conclude that the simplicity in the model reaction (7.1.1) we used in the previous chapters is reasonable as long as we are not concerned with the details of the structure of the wave front.

CHAPTER VIII

CONCLUSIONS

In the preceding chapters, using the MD method we found the following dynamical aspects of the exothermic reaction $A + S \rightarrow B + S + \Delta Q$.

1) The pattern formation processes. During the relaxation processes from the non-equilibrium state the spatial pattern formation processes were observed. It was found that they are similar to those in the phase transition phenomena in the alloy/spin systems. We investigated the nucleation and the growth processes and found that the growth law of the nucleus is different from that of the alloy/spin systems. Such difference originates from the difference in the driving mechanism of the domain boundary between the two systems. In our reaction system, the momentum flow at the boundary caused by the successive reactive collisions at the boundary sustains the propagation of the boundary.

2) The detonation propagation phenomena. It was demonstrated that our discretized description using particles can well reproduce the macroscopic features of the real detonation. The effects of the microscopic cluster which is caused by the fluctuations in particle number density distribution were also investigated. It was found that such microscopic fluctuations affect the detonation propagation velocity. Therefore we can say

that this is an example of the effects of the microscopic processes on the macroscopic phenomena.

3) Fluctuation dominated kinetics. We found that the fluctuations in density distribution dominate the evolution of the whole system in the late stage and lead it to the decay law different from the exponential decay law predicted by the rate equation. A simple analytical explanation of such fluctuation effects was suggested, which predicts a slower decay $\exp(-kt^{1/2})$ than exponential $\exp(-kt)$. We note that the MD experiments supported this result. The difference between the non-exothermic and the exothermic reactions was not detected in the fluctuation effects.

4) The effects of the activated complex with finite lifetime. Introducing an activated complex A^*, which has a finite lifetime, did not affect the essentials of the propagation mechanism of the detonation but changed the wave front structure of the detonation. This result indicates that our simple reaction model is a good approximation of the real exothermic reaction systems.

Despite the fact that our model system is a quite simple one, it shows various dynamical phenomena as were mentioned above. These phenomena will be common among the general exothermic reaction systems because we can expect that the essentials do not depend on the details of the reaction mechanism. For the simple model, in addition, we can perform a large scale MD experiments which gives us the information on the macroscopic phenomena. The macroscopic dynamics of the

chemically reacting systems in the non-equilibrium state have not been fully understood yet. The microscopic approach, such as the MD method, will become more and more important to gain deeper understanding of the chemical reaction systems.

REFERENCES

1) B. Otto, J. Schroeder and J. Troe: J. Chem. Phys. 81 (1984) 202.

2) G. Nicolis and I. Prigogine: Self-Organization in Nonequilibrium Systems (Wiley Interscience, New York, 1977).

3) F.A. Williams: Combustion Theory (Benjamin Cummings, 1985) 2nd ed.

4) R.A. Strehlow: Fundamentals of Combustion (International Textbook Company, Pennsylvania, 1968).

5) K. Kang and S. Redner: Phys. Rev. A32 (1985) 435.

6) B.J. Alder and T.E. Wainwright: J. Chem. Phys. 27 (1957) 1208.

7) B.J. Alder and T.E. Wainwright: Phys. Rev 127 (1962) 359.

8) B.J. Alder, D.M. Gass and T.E. Wainwright: J. Chem. Phys. 53 (1970) 3813.

9) A. Rahman: Phys. Rev. 136 (1964) A405.

10) L. Verlet: Phys. Rev. 159 (1967) 98.

11) M. Toda, H. Matsuda, Y. Hiwatari and M. Wadati: Structure and Properties of Liquids, (Iwanami,1976), (in Japanese).

12) D.L. Bunker and B.S. Jacobson: J. Am. Chem. Soc. 94 (1972) 1843.

13) A.J. Stace and J.N. Murrell: Mol. Phys. 33 (1977) 1.

14) J.N. Murrell, A.J. Stace and R. Dammel: J. Chem. Soc, Faraday Trans. II, 2 (1978) 1532.

15) A.H. Lipkus, F.P. Buff and M.G. Sceats: J. Chem. Phys. 79 (1983) 4830.

16) B.C. Freasier, D.L. Jolly and S. Nordholm: Chem. Phys. **82** (1983) 369.

17) G. Nicolis and A. Babloyantz: J. Chem. Phys. **51** (1969) 2632.

18) G. Nicolis: J. Stat. Phys. **6** (1972) 195.

19) Y. Kuramoto: Prog. Theor. Phys. **49** (1973) 1782.

20) A. Nitzan and J. Ross: J. Stat. Phys. **10** (1974) 379.

21) J. Portnow: Phys. Lett. **A51** (1975) 370.

22) P. Ortoleva and S. Yip: J. Chem. Phys. **65** (1976) 2045.

23) J.S. Turner: J. Phys. Chem. **81** (1977) 2379.

24) J. Boissonade and W. Horsthemke: Phys. Lett. **68A** (1978) 283.

25) J. Boissonade: Phys. Lett. **74A** (1979) 285.

26) J. Boissonade: Physica **113A** (1982) 607.

27) R. Der and S. Fritzsche: Chem. Phys. Lett. **121** (1985) 177.

28) M. Heinrichs and F.W. Schneider: Ber. Bunsenges. Phys. Chem. **87** (1983) 1195.

29) D.H. Tsai and S.F. Trevino: J. Chem. Phys. **79** (1983) 1684.

30) S.F. Trevino and D.H. Tsai: J. Chem. Phys. **81** (1984) 248.

31) D.H. Tsai and S.F. Trevino: J. Chem. Phys. **81** (1984) 5636.

32) M. Peyrard, S. Odiot, E. Oran, J. Boris and J. Schnur: Phys. Rev. **B33** (1986) 2350.

33) S.G. Lambrakos, E.S. Oran, J.P. Boris and R.H. Guirguis: in Shock waves in Condensed Matter 1987, ed. by S.C. Schmidt and N.C. Holmes (Elsevier Science Publishers B.V., 1988).

34) T. Kawakatsu, T. Matsuda and A. Ueda: J. Phys. Soc. Jpn. **57** (1988) 1191.

35) T. Kawakatsu and A. Ueda: J. Phys. Soc. Jpn. **57** (1988) 2955.

36) T. Kawakatsu and A. Ueda: submitted to J. Phys. Soc. Jpn.

37) T. Kawakatsu and A. Ueda in Computational Physics and Computational Chemistry: ed. by M. Tanaka and R. Yamamoto (Kaibundo, 1988) (in Japanese).

38) D.P. Chou and S. Yip: Comb. Flame 47 (1982) 215.

39) D.P. Chou and S. Yip: Comb. Flame 58 (1984) 239.

40) J. Gorecki and J. Gryko: J. Stat. Phys. 14 (1987) 329.

41) T. Kawakatsu and A. Ueda: J. Phys. Soc. Jpn. 56 (1987) 847.

42) S. Kanno: Prog. Theor. Phys. 79 (1988) 1330.

43) D. Toussaint and F. Wilczek: J. Chem. Phys. 78 (1983) 2642.

44) L.W. Anacker and R. Kopelman: Phys. Rev. Lett. 58 (1987) 289.

45) A.G. Vitukhnovsky. B.L. Pyttel and I.M. Sokolov: Phys. Lett. 128 (1988) 161.

46) S. Kanno: Prog. Theor. Phys. 79 (1988) 721.

47) B.Ya Balagurov and V.G. Vaks: Sov. Phys. JETP 38 (1974) 968.

48) P. Grassberger and I. Procaccia: J. Chem. Phys. 77 (1982) 6281.

49) R.F. Kayser and J.B. Hubbard: Phys. Rev. Lett. 51 (1983) 79.

50) T. Kawakatsu and A. Ueda: in preparation.

51) Monte Carlo Methods (2nd ed.): ed. by K. Binder (Springer-Verlag,1986)

52) M.P. Allen and D.J. Tildesley: Computer Simulation of Liquids (Oxford Science Publications, 1987).

53) H. Haken: Synergetics ; an Introduction, (Springer-Verlag, 1977).

54) H. Haken: Advanced Synergetics, (Springer-Verlag, 1983).

55) D.C. Rapaport: Phys. Rev. Lett. 60 (1988) 2480.

56) J.W. Cahn: Trans. Metal. Soc. AIME 242 (1968) 166.

57) F.H. Ree and W.G. Hoover: J. Chem. Phys. 40 (1964) 939.

58) J.L. Finny: J. Compt. Phys. 32 (1979) 137.

APPENDICES

Appendix A

Here, we give a brief derivation of Rankine-Hugoniot equation for our reactive system.

As was presented in chapter IV, Rankine-Hugoniot equation for a steady detonation wave is described as follows:

$$\frac{1}{2}(P_2 - P_1)(V_2 + V_1) = Nk_B(T_2 - T_1) + (P_2V_2 - P_1V_1) - q \qquad (A.1)$$

Here, the quantities P, V, N and T represent pressure, volume per unit mass, total number of particles per unit mass and temperature, respectively. Subscripts 1 and 2 represent the upper stream and the down stream region of the wave. The parameter q is the released chemical energy during the change from state 1 to state 2. When the initial state (state 1) is composed of A and S particles, whose numbers are in the ratio c_R : $1-c_R$, the equilibrium number of created B particles in state 2 is given by

$$N_B = \frac{c_R N}{1 + \exp(-\Delta Q/k_B T_2)} \cdot \qquad (A.2)$$

As the released chemical energy q is given by $q = N_B \Delta Q$, Rankine-Hugoniot equation (A.1) becomes to

$$(P_2 + P_1)(V_2 - V_1) + 2Nk_B(T_2 - T_1) = \frac{2c_R N\Delta Q}{1 + \exp(-\Delta Q/k_B T_2)} \cdot \qquad (A.3)$$

With use of this Rankine-Hugoniot equation, eq. (A.3), we evaluated the stable detonation velocity. The procedure for obtaining the detonation velocity is described in chapter IV.

Appendix B

If we assume the velocity distribution function of particles to be a 2-dimensional Maxwell-Boltzmann one, the distribution function of the magnitude of the relative velocity $g = |\vec{v}_2 - \vec{v}_1|$ is given by

$$f(g)\, dg = \frac{m}{2k_BT}\, g\, \exp\left(- \frac{m}{4k_BT}\, g^2 \right) dg. \qquad (B.1)$$

If we denote the impact parameter as b, the condition that a forward reaction takes place is as follows:

$$\frac{m}{4}\, g^2 \left\{ 1 - \left(\frac{b}{\sigma}\right)^2 \right\} \geq \varepsilon. \qquad (B.2)$$

Assuming a uniform distribution of b within a section of $[\, -\sigma, \sigma\,]$ as

$$f(b) = \begin{cases} 1/(2\sigma) & -\sigma \leq b \leq \sigma \\ 0 & \text{otherwise}, \end{cases} \qquad (B.3)$$

the probability of the occurrence of a reaction at a reactive-type collision is

$$P_R = \iint_D dg\, db\, f(g)\, f(b), \qquad (B.4)$$

where D means the domain in (g,b) plane in which the condition (B.2) is satisfied. From eq. (B.4) we obtain eq. (5.4.3).

LIST OF PUBLICATIONS

1) T. Munakata and T. Kawakatsu; J. Chem. Phys. 80 (1984) 2800.
"Velocity field and self-diffusion in liquid binary mixtures. A generalized Stokes-Einstein relation"

2) T. Kawakatsu and T. Munakata; Prog. Theor. Phys. 74 (1985) 11.
"Kink dynamics in a one-dimensional conserved TDGL system"

3) T. Munakata and T. Kawakatsu; Prog. Theor. Phys. 74 (1985) 262.
"Resonance in non-Markovian activation processes"

4) T. Kawakatsu and A. Ueda; J. Phys. Soc. Jpn. 56 (1987) 847.
"A molecular dynamics study of the nucleation and growth process in an exothermically reacting system"

5) T. Kawakatsu, T. Matsuda and A. Ueda; J. Phys. Soc. Jpn. 57 (1988) 1191.
"A molecular dynamics study of an exothermically reacting system; A detonation phenomenon"

6) T. Kawakatsu and A. Ueda; J. Phys. Soc. Jpn. 57 (1988) 2955.
"A molecular dynamics study of relaxation processes at a detonation Wave front"

7) T. Kawakatsu and A. Ueda; submitted to J. Phys. Soc. Jpn.
"A molecular dynamics study of an exothermically reacting system; The effects of the finite lifetime activated complex on the structure of the detonation wave front"

8) T. Kawakatsu and A. Ueda; in Computational Physics and Computational Chemistry, ed. by M. Tanaka and R. Yamamoto (Kaibundo, 1988) (in Japanese).
"Molecular dynamics studies of the condensed phase chemical reaction systems"

This thesis is composed of the papers 4-8.